Geological Magazine

www.cambridge.org/geo

Original Article

Cite this article: Li X-Y, Li S-Z, Huang F, Wang Y-M, Yu S-Y, Cao H-H, and Xie W-M (2019) Petrogenesis of high Ba–Sr plutons with high Sr/Y ratios in an intracontinental setting: evidence from Early Cretaceous Fushan monzonites, central North China Craton. *Geological Magazine* **156**: 1965–1981. https://doi.org/10.1017/S0016756819000256

Received: 6 September 2018
Revised: 3 March 2019
Accepted: 11 March 2019
First published online: 13 June 2019

Keywords:
Cretaceous; high Ba–Sr pluton; high Sr/Y; monzonite; North China Craton; petrogenesis

Author for correspondence: San-Zhong Li,
Email: Sanzhong@ouc.edu.cn

CAMBRIDGE UNIVERSITY PRESS

Petrogenesis of high Ba–Sr plutons with high Sr/Y ratios in an intracontinental setting: evidence from Early Cretaceous Fushan monzonites, central North China Craton

Xi-Yao Li[1,2], San-Zhong Li[1,2,*], Feng Huang[3], Yong-Ming Wang[4], Sheng-Yao Yu[1,2], Hua-Hua Cao[1,2] and Wei-Ming Xie[5]

[1]Key Lab of Submarine Geosciences and Prospecting Techniques, MOE, Institute for Advanced Ocean Study, College of Marine Geosciences, Ocean University of China, Qingdao 266100, China; [2]Laboratory for Marine Geology and Environment, Qingdao National Laboratory for Marine Science and Technology, Qingdao 266237, China; [3]School of Earth Science and Resources, China University of Geosciences, Beijing 100083, China; [4]School of Earth and Space Exploration, Arizona State University, Tempe, AZ 85287-1404, USA and [5]Hebei Institute of Geological Survey, Shijiazhuang 050081, China

Abstract

Geochronological, major and trace element, and Sr–Nd–Hf isotopic data are reported for the monzonitic rocks of the Fushan pluton in the Taihang Mountains, central North China Craton, in order to investigate their sources, petrogenesis and tectonic implications. Zircon U–Pb dating results reveal that the Fushan pluton was emplaced during the Early Cretaceous (~126–124 Ma). The monzonites and quartz monzonites are mainly characterized by calc-alkaline and magnesian features and display light rare earth element (LREE) enrichment and flat heavy REE (HREE) patterns with slightly positive Eu anomalies. They have similar whole-rock initial $^{87}Sr/^{86}Sr$ ratios (0.70653–0.70819), $\varepsilon_{Nd}(t)$ values (−13.6 to −18.6) and zircon $\varepsilon_{Hf}(t)$ values (−21.8 to −17.3). The primary magma of the Fushan pluton was derived from the partial melting of a spinel-facies amphibole-bearing ancient enriched lithospheric mantle. The monzonitic rocks also have high Ba–Sr and low Y and Yb contents, with high Sr/Y and La/Yb ratios. These geochemical features of monzonitic rocks are not only inherited from the magma source but also significantly enhanced by crystal fractionation during magmatic evolution; e.g. hornblende fractionation increased the Ba–Sr concentrations and Sr/Y ratios. During the Early Cretaceous, the slab sinking and roll-back of the Palaeo-Pacific Plate could have created an ancient big mantle wedge beneath East Asia and induced a lithospheric extensional process in the central North China Craton within an intracontinental setting.

1. Introduction

Magma generation and processes play important roles in the material differentiation of the Earth and the continental crust (Rudnick, 1995; Foley *et al.* 2002). The course of magma from its source to intrusion into wall rock usually involves several petrogenetic processes, e.g. the partial melting of a source, assimilation and fractional crystallization, which contribute to the compositional diversity of magmas and associated rocks (Depaolo, 1981; Spera & Bohrson, 2001; Annen *et al.* 2005). Intrusive complexes or batholiths with distinctive geochemical signatures, such as high Sr/Y and high Ba–Sr signals, have attracted great attention, with significant implications for petrogenesis and tectonics (Drummond & Defant, 1990; Fowler *et al.* 2001). High Sr/Y magmatic rocks usually have adakitic signatures (high Sr and low Y and Yb concentrations with high Sr/Y and La/Yb ratios), which are related to continental crustal evolution and recycling, specific geodynamics and porphyry-type Cu ± Mo ± Au deposits (Xu *et al.* 2002; Martin *et al.* 2005; Castillo, 2012). Meanwhile, high Ba–Sr intrusions usually vary from appinite to granite and are characterized by high alkali, Ba–Sr and light rare earth element (LREE) concentrations and low heavy REE (HREE) concentrations, carrying important information on their petrogenesis and geodynamics in orogenic belts or subduction zones (Tarney & Jones, 1994; Fowler *et al.* 2008; Bruand *et al.* 2014; Pan *et al.* 2016; Zhu *et al.* 2018).

The North China Craton (NCC) is one of the most important regions when studying the complicated evolution of the continental lithosphere, as this region experienced craton destruction during the Phanerozoic (Wu *et al.* 2005; Xu, 2007; Zheng *et al.* 2007a; Zhang, 2009). The Cretaceous Period is considered as the major time of intense magmatism and mineralization in the NCC (Xu *et al.* 2009a; Zhu *et al.* 2012). These Cretaceous magmatic rocks are complex products of multiple sources, e.g. asthenospheric mantle, enriched lithospheric mantle, ancient basement, and reworked and juvenile crustal materials (Zhang *et al.* 2005; Yang *et al.* 2010;

Chen *et al.* 2013; Huang *et al.* 2017). More significantly, high Sr/Y magmatic rocks and high Ba–Sr intrusions have been found in the central and eastern NCC during the Cretaceous Period (Zhang *et al.* 2001; Qian *et al.* 2002; Wang *et al.* 2014; Ma *et al.* 2016*a*; Wang *et al.* 2017). These high Sr/Y magmatic rocks in the NCC usually show adakitic features that imply their special genetic and geodynamic links to a subducted oceanic slab (Wang *et al.* 2016*a*), thickened or delaminated lower continental crust (Gao *et al.* 2004; Liu *et al.* 2012; Xu *et al.* 2013; Yang *et al.* 2016), fractional crystallization processes (Gao *et al.* 2012; Ma *et al.* 2016*b*), or inheritance from source materials at the normal crustal level (Qian & Hermann, 2010; Jiang *et al.* 2011; Ma *et al.* 2015). Meanwhile, the Cretaceous high Ba–Sr intrusions in the NCC are related to the partial melting of the enriched subcontinental lithospheric mantle and subsequent crust–mantle interaction (Wang *et al.* 2017) or the mixing of melts from the basement and juvenile mafic lower crust (Wang *et al.* 2014) and are possibly linked to the post-collisional lithospheric extension (Qian *et al.* 2002) or subduction of the Palaeo-Pacific Plate (Wang *et al.* 2014).

In the southern Taihang Mountains, the eastern part of the central NCC, a series of Early Cretaceous intrusions crop out, varying from mafic to intermediate and felsic rocks (Wang *et al.* 2006; Chen *et al.* 2008; Xu *et al.* 2009b; Ying *et al.* 2011), and some of these intrusions have genetic relationships with skarn-type iron deposits (Zheng *et al.* 2007b; Shen *et al.* 2013; Deng *et al.* 2015). Each intrusive complex shows a certain rock association, e.g. monzogabbro–monzonite, monzonite–quartz monzonite and syenite–granite (Chen *et al.* 2004; Sun *et al.* 2015). The petrogenesis of these intrusions and related geodynamic processes beneath the central NCC during the Early Cretaceous are still controversial, such as magmatic mixing (Chen *et al.* 2009), fractionation of a water-saturated magma (Gao *et al.* 2013; Wang *et al.* 2017), mantle-derived magmas involving delaminated lower continental crust (Xu *et al.* 2009b; Sun *et al.* 2014) or assimilation of peridotite by monzodiorite magma at crustal depths (Qian & Hermann, 2010). Then, the source, petrogenesis and tectonic implications of the Early Cretaceous intrusive rocks in the southern Taihang Mountains are still not completely known. In this paper, we present petrological, zircon U–Pb–Hf isotopic and whole-rock elemental and Sr–Nd isotopic geochemical data for the monzonites and quartz monzonites of the Early Cretaceous Fushan pluton, southern Taihang Mountains, with the aim of constraining their geochronology and petrogenesis and giving implications for their tectonic setting.

2. Geological background and samples

The NCC is mainly composed of Archaean–Palaeoproterozoic metamorphic basement and Proterozoic to Cenozoic covers (Zhao & Cawood, 2012) and is bounded to the north by the Central Asian orogenic belt and to the south and east by the Qinling–Dabie–Sulu orogenic belt (Li *et al.* 2018*a*) (Fig. 1a). The central NCC is an important transitional region between the eastern and western parts of the NCC, approximately overlapping the geological Palaeoproterozoic Trans-North China Orogen and geophysical North–South Gravity Lineament (NSGL). The Trans-North China Orogen is a Palaeoproterozoic orogenic belt formed by the amalgamation of the eastern and western blocks of the NCC (Zhao & Cawood, 2012). The NSGL is a geophysical boundary between the eastern and western parts of the NCC and separates two topographically, tectonically and seismically different regions (Xu, 2007). In the central NCC, there are several Archaean–Palaeoproterozoic basements, e.g. the Wutai and Zanhuang complexes in the Taihang Mountains, which are dominantly composed of schist, gneiss, amphibolite, marble and banded iron formations (Zhao & Cawood, 2012). After a long period of stability, intense structural deformation developed in the central NCC during the late Middle Jurassic, with many NE-trending folds and thrust faults, and the directions of tectonic lines converted from the previous E–W to the NE-NNE direction (Li *et al.* 2015). Meanwhile, voluminous late Mesozoic magmatic intrusions are exposed in the regions of the Taihang Mountains, central NCC, such as the Han–Xing and Fuping–Wutai districts (Chen *et al.* 2004). The Han–Xing district in the south Taihang Mountains is mainly composed of diorite, monzonite and syenite, and the Fuping–Wutai district in the north Taihang Mountains is mainly composed of monzonitic granite and granodiorite (Gao *et al.* 2013; Li *et al.* 2014; Sun *et al.* 2015).

The Han–Xing district, which is named after two cities (Handan and Xingtai), has outcrops of an Archaean–Proterozoic basement covered by unmetamorphosed Palaeozoic limestones that are intruded by a number of dioritic and monzonitic plutons (Fig. 1b). The Han–Xing district is famous for its numerous iron skarn deposits along the contact belts between the Mesozoic intrusions and Middle Ordovician carbonate rocks (Zheng *et al.* 2007b; Shen *et al.* 2013). The Mesozoic magmatic belt in this district is mainly composed of the Fushan, Wu'an and Hongshan intrusive complexes (Chen *et al.* 2004). The Fushan intrusive rocks are composed of monzogabbro, diorite, monzonite and quartz monzonite. The Wu'an intrusive rocks are mainly composed of diorite, monzonite and quartz monzonite, and the Hongshan pluton includes syenite and granite.

The studied samples were collected from the Fushan pluton, including monzonite and quartz monzonite (Figs. 1c and 2a). The monzonite samples are medium-grained and consist of hornblende (20–30 vol. %), plagioclase (35–45 vol. %), K-feldspar (20–30 vol. %), Fe–Ti oxides (<10 vol. %) and a few accessory minerals, e.g. zircon and apatite (Fig. 2b, c). The quartz monzonites are also medium-grained and consist of plagioclase (40–50 vol. %), K-feldspar (25–30 vol. %), quartz (<10 vol. %), hornblende (<15 vol. %), Fe–Ti oxides (<5 vol. %) and a few accessory minerals, e.g. zircon and apatite (Fig. 2d).

3. Analytical methods

3.a. Zircon U–Pb dating and Lu–Hf isotope analyses

The zircon grains were separated by density and magnetic techniques followed by hand-picking under a binocular microscope. Cathodoluminescence (CL) imaging was performed by a JEOL (JSM-6510) scanning electron microscope fitted with a Gatan MiniCL detector to show the internal structures. *In situ* zircon U–Pb dating was conducted by laser ablation inductively coupled plasma mass spectrometry (LA-ICP-MS) at the Testing Center of Shandong Bureau, China Metallurgical Geology Bureau (Jinan, China). A Thermo Scientific iCAP™ Q ICP-MS instrument was equipped with a GeoLasPro 193 nm ArF Excimer Laser (Coherent Inc.) laser ablation system. The diameter of the laser ablation craters was 32 μm. The analytical procedure and precision are described by Li *et al.* (2018*b*), and the detailed procedures follow Liu *et al.* (2010). The zircon standard Plešovice (337 ± 0.37 Ma) (Sláma *et al.* 2008) was used as an external standard.

The *in situ* zircon Lu–Hf isotopes were measured using a Neptune Plus Multi-Collector ICP-MS (MC-ICP-MS, Thermo Fisher) in combination with a GeoLas HD 193 excimer ArF laser ablation system at the Guangxi Key Laboratory of Hidden Metallic Ore Deposits Exploration, Guilin University of Technology (Guilin, China). The detailed analytical procedures, precision and data calibration are described by Huang *et al.* (2016). The analytical spots used a beam size of 45 μm, and the standard zircon GJ-1 was used to evaluate the reliability of the analytical data, which yielded a weighted mean $^{176}Hf/^{177}Hf$ ratio of 0.282006 ± 0.000004 (2σ, $n = 20$). This value was in good agreement with the recommended value (0.282000 ± 0.000005, Morel *et al.* 2008). The $\varepsilon_{Hf}(t)$ values were calculated using chondritic ratios of $^{176}Hf/^{177}Hf = 0.282785$ and $^{176}Lu/^{177}Hf = 0.0336$ (Bouvier *et al.* 2008) and a decay constant λ for ^{176}Lu of 1.865×10^{-11} a^{-1} (Scherer *et al.* 2001). The single-stage Hf model ages (T_{DM1}) were calculated based on a depleted mantle source with $^{176}Hf/^{177}Hf = 0.28325$ and $^{176}Lu/^{177}Hf = 0.0384$ (Vervoort & Blichert-Toft, 1999), the two-stage Hf model ages (T_{DM2})

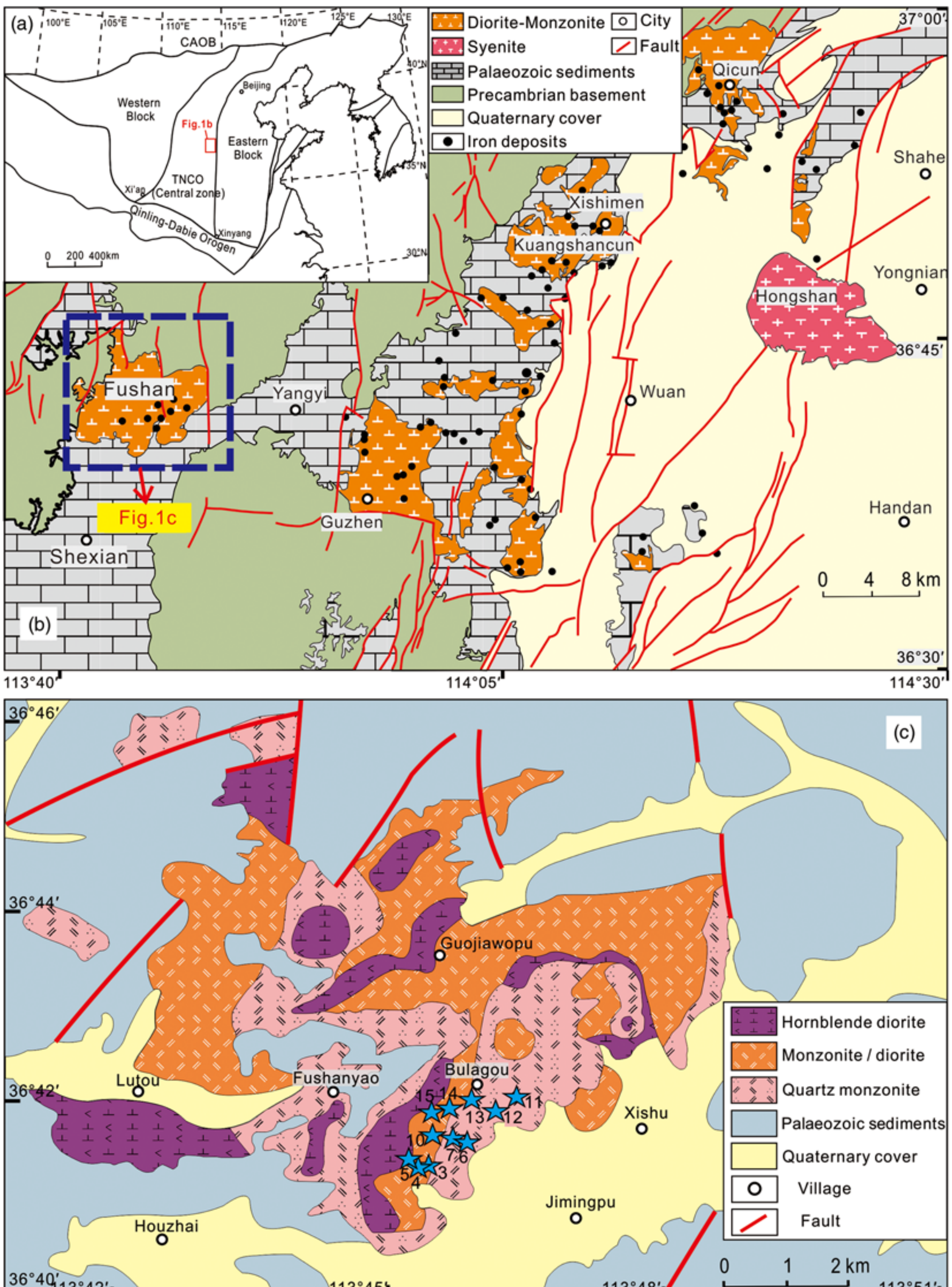

Fig. 1. (Colour online) (a) Tectonic units of the North China Craton (after Zhao & Cawood, 2012); (b) distribution of Mesozoic magmatic intrusions in the southern Taihang Mountains (after Sun *et al.* 2015); (c) geological map of the Fushan pluton (modified after a 1:25 000 geological map of Changzhi City and its peripheral area, 2008).

https://doi.org/10.1017/S0016756819000256 Published online by Cambridge University Press

were calculated using an average continental crustal value ($^{176}Lu/^{177}Hf = 0.015$) (Griffin *et al.* 2002), and the evolution of the lower mafic crust using a value of $^{176}Lu/^{177}Hf = 0.022$ (Amelin *et al.* 1999).

3.b. Major and trace element and Sr–Nd isotope analyses

The whole-rock major and trace element compositions were analysed at the Testing Center of Shandong Bureau, China Metallurgical Geology Bureau. For the major element analyses, the prepared samples were fused using a lithium tetraborate ($Li_2B_4O_7$) – lithium metaborate ($LiBO_2$) – lithium fluoride (LiF) flux with a fluxing agent of lithium bromide (LiBr). The resultant fused disc was measured by X-ray fluorescence spectrometry (XRF, ARL 9900XP instrument) for the major element compositions, with analytical precision and accuracy better than 5 %. For the trace element analyses, the sample powders (~100 mg, <200 mesh) were digested in Teflon bombs by hydrofluoric and nitric acids (3 mL HF and 2 mL HNO_3) and heated in an oven for 48 hours at ~185 °C. Then, the solution was evaporated to dryness at ~130 °C, 2 mL HNO_3 was added and the solution was distilled to dryness again. After drying, 1.5 mL HNO_3 and 1.5 mL ultrapure water were added for redissolution, and the solution was heated in a bomb at ~180 °C for 12 hours and then the final solution was diluted to 100 mL. The trace elements were measured by a Thermo X Series 2 ICP-MS, and the analytical accuracies were better than 10 %.

Whole-rock Sr–Nd isotope analyses were performed on a Finnigan MAT-262 thermal ionization mass spectrometer (TIMS) at the Key Laboratory of Crust–Mantle Materials and Environments, Chinese Academy of Sciences, University of Science and Technology of China (Hefei, China). The sample powders (~100 mg, <200 mesh) for the Sr–Nd isotopic analyses were dissolved in $HClO_4$–HF for ~7 days in Teflon screw-cap beakers at ~200 °C. Details of the separation and concentration of Sr, Nd and REEs and the analytical techniques are given in Chen *et al.* (2002). The measured data were normalized to $^{86}Sr/^{87}Sr = 0.1194$ and $^{146}Nd/^{144}Nd = 0.7219$ (Thirlwall, 1991). The measured $^{87}Sr/^{86}Sr$ ratios were 0.710247 ± 0.000012 (2σ, $n = 6$) for the NBS987 standard and 0.703983 ± 0.000009 (2σ, $n = 3$) for the AGV-2 standard. The measured $^{143}Nd/^{144}Nd$ ratios were 0.512116 ± 0.000009 (2σ, $n = 6$) for the Jndi-1 standard, and 0.512793 ± 0.000010 (2σ, $n = 3$) for the AGV-2 standard.

4. Results

4.a. Zircon U–Pb ages

The zircon U–Pb dating results are listed in Supplementary Table S1 in the online Supplementary Material (available at https://doi.org/10.1017/S0016756819000256). Zircon grains from a monzonite sample (QS35-14) are euhedral to subhedral and display oscillatory zoning (Fig. 3a), which is typical of magmatic zircon. Twenty-eight analytical spot analyses were obtained on 28 zircon grains. These analyses record 191–1000 ppm Th, 140–454 ppm U and high Th/U ratios (1.0–2.2). The zircons are concordant with $^{206}Pb/^{238}U$ ages of 126.1–127.7 Ma, yielding a weighted mean $^{206}Pb/^{238}U$ age of 126.8 ± 1.2 Ma (MSWD = 0.023, $n = 28$) (Fig. 3b). This age is interpreted as the crystallization age of the monzonite.

Zircon grains from a quartz monzonite sample (QS35-6) are also euhedral to subhedral and display oscillatory zoning (Fig. 3c), typical for magmatic zircon. Twenty-two analytical spot analyses

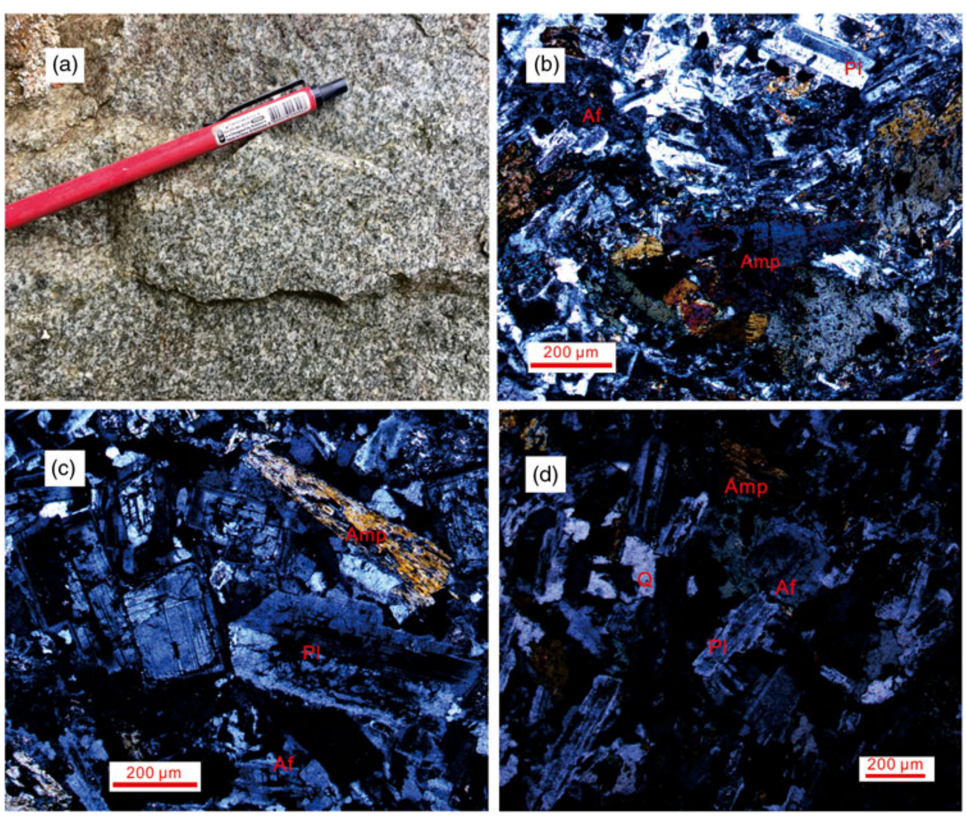

Fig. 2. (Colour online) (a) Macroscopic image of monzonitic rocks. (b–d) Photomicrographs of representative samples (cross-polarized light): (b) monzonite (QS35-10); (c) monzonite (QS35-4); (d) quartz monzonite (QS35-11). (Amp = amphibole, Q = quartz, Af = alkali-feldspar, Pl = plagioclase.)

https://doi.org/10.1017/S0016756819000256 Published online by Cambridge University Press

were obtained on 22 zircon grains and record 165–3377 ppm Th and 167–1088 ppm U with high Th/U ratios (1.0–3.1). The zircons show concordant $^{206}Pb/^{238}U$ ages ranging from 123.7 to 125.7 Ma, yielding a weighted average of 124.6 ± 1.5 Ma (MSWD = 0.022, $n = 22$) (Fig. 3d). This age is interpreted as the formation age of the quartz monzonite.

4.b. Major and trace elements

The whole-rock major and trace element data for the samples are listed in Supplementary Table S2 in the online Supplementary Material (available at https://doi.org/10.1017/S0016756819000256). The geochemical compositions of the samples fall mainly into the range of monzonite and quartz monzonite on the TAS (total alkali silica) diagram (Fig. 4a). The monzonite samples have intermediate SiO_2 (55.71–61.31 wt %) and high K_2O and Na_2O contents, showing calc-alkaline, magnesian ($FeO^T/(FeO^T + MgO)$ values of 0.5–0.7) and peraluminous to metaluminous features with A/CNK values ($Al_2O_3/(CaO + K_2O + Na_2O)$ mole ratio) of 0.97–1.11 and A/NK values ($Al_2O_3/(K_2O + Na_2O)$ mole ratio) of 1.38–1.76 (Fig. 4b, c, d). The monzonites have high $Fe_2O_3{}^T$ (4.04–8.44 wt %), MgO (2.79–6.05 wt %) and CaO contents and moderate Al_2O_3, TiO_2 and P_2O_5 contents (Fig. 5). The quartz monzonites (SiO_2, 63.06–65.05 wt %) display variable geochemical features with the monzonites, e.g. calc-alkaline to alkalic, magnesian to ferroan, and metaluminous characteristics (A/CNK values of 0.7–0.8; A/NK values of 1.4–1.8) (Fig. 4b, c, d). The quartz monzonites have higher SiO_2 and Al_2O_3 and lower MgO (0.29–1.93 wt %), $Fe_2O_3{}^T$ (1.98–4.27 wt %), CaO, TiO_2 and P_2O_5 contents than the monzonites (Fig. 5). They also show lower Cr (6–26 ppm), Ni (4–10 ppm) and V (34–74 ppm) concentrations than those of the monzonites (Cr = 23–257 ppm, Ni = 10–88 ppm and V = 117–163 ppm).

The trace element compositions of the monzonites and quartz monzonites are similar. Their chondrite-normalized REE patterns show enrichment in LREEs and nearly flat HREE patterns ($(La/Yb)_N = 10–24$; $(La/Sm)_N = 3.3–6.8$; $(Gd/Yb)_N = 1.8–2.3$), with slightly positive Eu anomalies (Eu/Eu* = 1.0–1.2) (Fig. 6a, b). In the primitive mantle-normalized spider diagram (Fig. 6c, d), most samples show significant enrichment in Ba and Sr and depletion in Nb and Ta with variable Rb depletion.

4.c. Sr–Nd isotopes

The whole-rock Sr–Nd isotope compositions of the samples are listed in Supplementary Table S3 in the online Supplementary Material (available at https://doi.org/10.1017/S0016756819000256). The initial $^{87}Sr/^{86}Sr$ ratios and $\varepsilon_{Nd}(t)$ values are calculated using

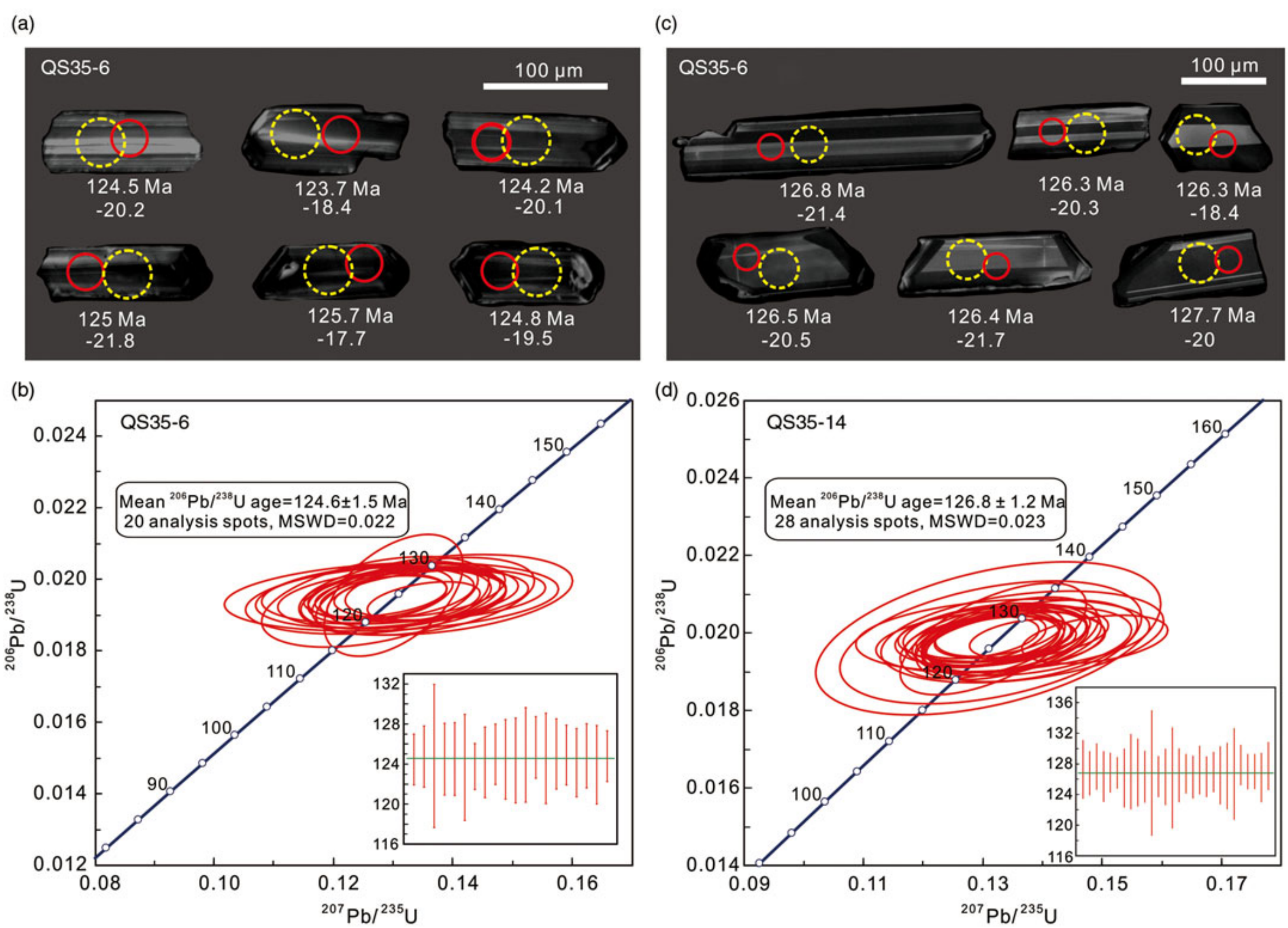

Fig. 3. (Colour online) CL images of representative zircons and zircon U–Pb concordia diagrams. (a, b) Monzonite sample (QS35-14); (c, d) quartz monzonite sample (QS35-6). Red solid circles indicate U–Pb dating spots, whereas yellow dashed circles indicate Hf isotope analysis spots. Ages and $\varepsilon_{Hf}(t)$ values are also shown for each spot.

their zircon U–Pb ages obtained in this study. The monzonites show calculated initial $^{87}Sr/^{86}Sr$ ratios ranging from 0.70653 to 0.70763 and $\varepsilon_{Nd}(t)$ values ranging from −13.6 to −17.6 (Fig. 7), with two-stage Nd model ages (T_{DM2} (Nd)) of 1.7–2.0 Ga. The quartz monzonites have similar $\varepsilon_{Nd}(t)$ values (−15.6 to −18.6) and higher initial $^{87}Sr/^{86}Sr$ ratios (0.70766–0.70819) than the monzonites, with T_{DM2} (Nd) ages of 1.9–2.1 Ga.

4.d. Zircon Hf isotopes

The zircon Lu–Hf isotope compositions are listed in Supplementary Table S4 in the online Supplementary Material (available at https://doi.org/10.1017/S0016756819000256). The zircon grains from the monzonite (sample QS35-14) have calculated initial $^{176}Hf/^{177}Hf$ ratios of 0.282077–0.282205 and $\varepsilon_{Hf}(t)$ values of −21.8 to −17.3 (Fig. 8). The zircons show depleted mantle model ages (T_{DM1} (Hf)) of 1.7–1.5 Ga and two-stage Hf model ages (T_{DM2}(Hf)) of 2.5–2.2 Ga. The zircon grains from the quartz monzonite (sample QS35-6) have initial $^{176}Hf/^{177}Hf$ ratios (0.282076–0.282189), $\varepsilon_{Hf}(t)$ values (−21.8 to −17.8), T_{DM1} (Hf) ages (1.7–1.5 Ga) and T_{DM2} (Hf) ages (2.5–2.3 Ga) similar to those of the monzonite sample.

5. Discussion

5.a. Timing of Early Cretaceous magmatism in the Han–Xing district

The zircon U–Pb dating of the monzonite (QS35-14) and quartz monzonite (QS35-6) samples yields emplacement ages in the Early Cretaceous, 126 ± 1 Ma and 124 ± 1 Ma, respectively. The previous geochronological studies, e.g. whole-rock Rb–Sr and mineral K–Ar dating, show scattered ages (~218–63 Ma, summarized by Sun *et al.* (2015)) for the Mesozoic intrusions from the Han–Xing district and adjacent regions in the southern Taihang Mountains, central NCC. Recently, more precise dating results, e.g. zircon U–Pb and mineral $^{40}Ar–^{39}Ar$ dating, have been conducted for these igneous rocks. In the Fushan pluton, the zircon U–Pb dating of the intrusive rocks mainly yields emplacement ages of ~128–125 Ma (Peng *et al.* 2004; Xu *et al.* 2009b; Deng *et al.* 2015). In the Wu'an complexes, zircon U–Pb dating shows that the diorite and monzonite were emplaced ~134–127 Ma (Chen *et al.* 2008; Deng *et al.* 2015; Sun *et al.* 2014, 2015). In the Hongshan pluton, the zircon U–Pb dating of the syenite shows emplacement ages of ~135–130 Ma (Chen *et al.* 2008; Sun *et al.* 2015) and a Rr–Sr

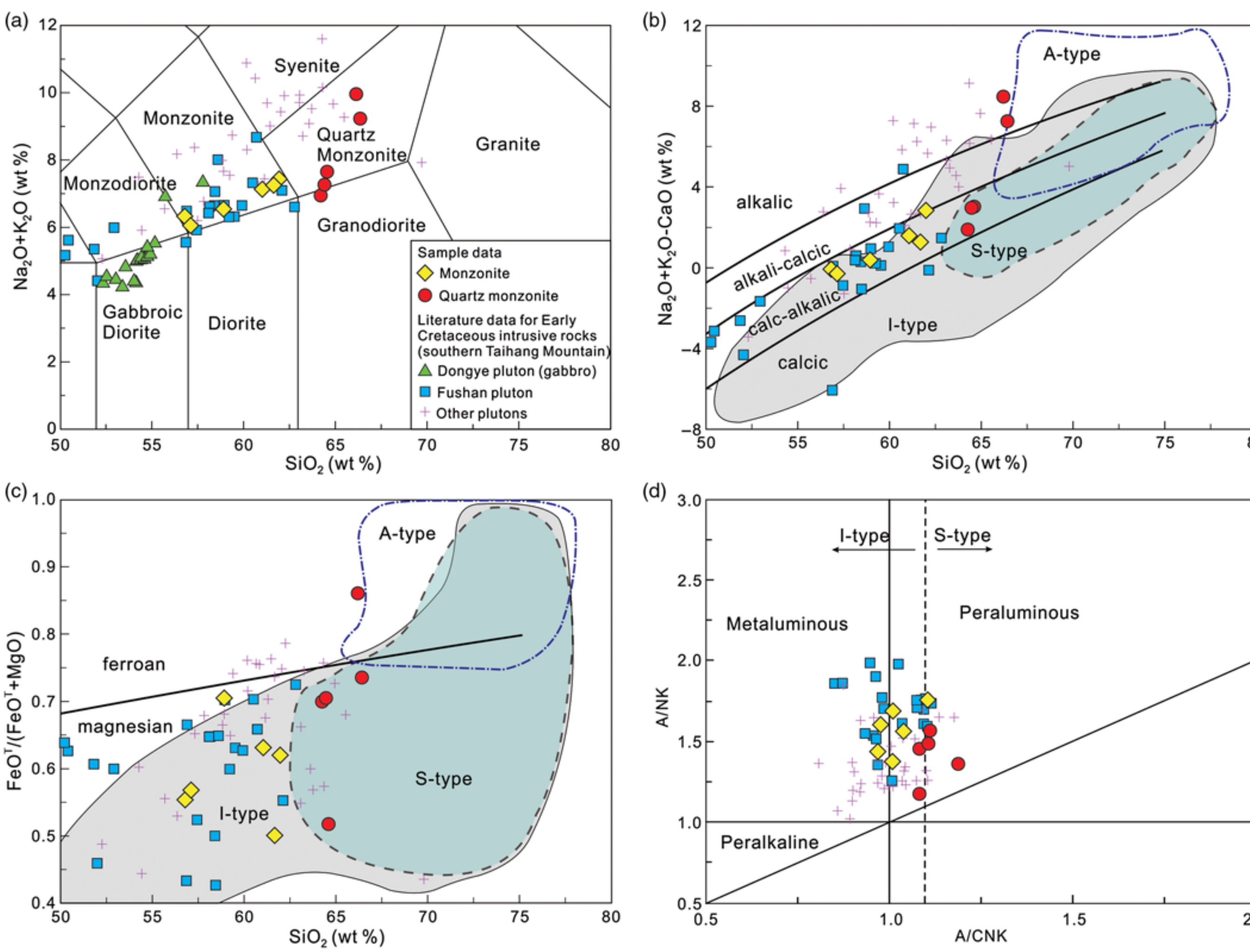

Fig. 4. (Colour online) (a) ($K_2O + Na_2O$) vs SiO_2 (TAS; after Le Maitre, 2002); (b) A/CNK vs A/NK (after Maniar & Piccoli, 1989); (c) $FeO^T/(FeO^T + MgO)$ vs SiO_2; and (d) ($Na_2O + K_2O$–CaO) vs SiO_2 (after Frost *et al.* 2001). All samples were normalized to 100 % after excluding the loss on ignition (LOI). A/CNK = $Al_2O_3/(CaO + Na_2O + K_2O)$ in mole ratio; A/NK = $Al_2O_3/(Na_2O + K_2O)$ in mole ratio. Data sources: Early Cretaceous intrusive rocks in the southern Taihang Mountains: Dongye pluton (gabbro) (Wang *et al.* 2006), Fushan pluton (Dong *et al.* 2003; Chen *et al.* 2004; Peng *et al.* 2004; Xu *et al.* 2009b) and other plutons (Chen *et al.* 2004; Sun *et al.* 2014, 2015).

https://doi.org/10.1017/S0016756819000256 Published online by Cambridge University Press

isochron age of ~138 Ma (Chen *et al.* 2008; Sun *et al.* 2015). The Early Cretaceous gabbroic rocks in the southern Taihang Mountains were emplaced ~125 Ma (Wang *et al.* 2006). The Early Cretaceous intrusions in the adjacent regions of the Handan–Xingtai district, southern Taihang Mountains, show similar ages of ~131–118 Ma (Peng *et al.* 2004; Ying *et al.* 2011; Li *et al.* 2014; Wang *et al.* 2017). Meanwhile, the hydrothermal zircon U–Pb and phlogopite $^{40}Ar–^{39}Ar$ dating for magnetite-bearing skarns yields ages ranging from 137 to 129 Ma, which implies that the timing of the iron skarn mineralization is consistent with the

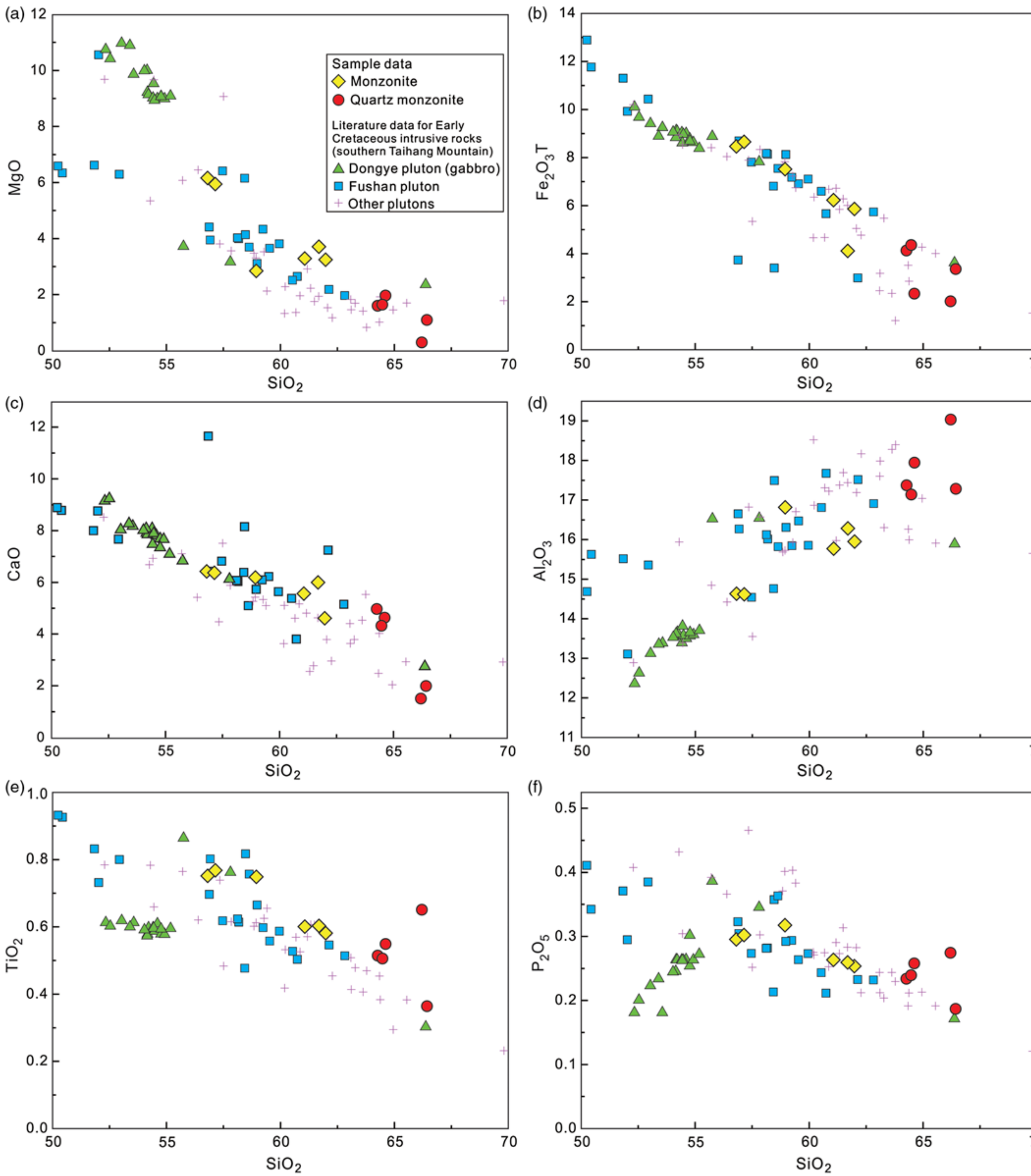

Fig. 5. (Colour online) Variations in (a) SiO_2 vs MgO, (b) $Fe_2O_3^T$, (c) Al_2O_3, (d) CaO, (e) Na_2O, (f) TiO_2. All samples were normalized to 100 % after excluding LOI. Data sources as shown in Figure 4.

https://doi.org/10.1017/S0016756819000256 Published online by Cambridge University Press

emplacement ages of the ore-related intrusions in the Handan–Xingtai district (Zheng *et al.* 2007b; Shen *et al.* 2013; Deng *et al.* 2015). In addition, previous geochronological studies show that the late Mesozoic magmatism in the eastern NCC mainly happened in the Early Cretaceous (~136–115 Ma) time with a giant igneous event (Wu *et al.* 2005; Zhang *et al.* 2014). Then, intense late Mesozoic magmatic activity concentrated in the Han–Xing district and adjacent regions, southern Taihang Mountains, developed in the Early Cretaceous (~138–118 Ma).

5.b. Petrogenesis of monzonites and quartz monzonites

5.b.1. Crustal contamination and fractional crystallization

The Fushan pluton intruded into the Upper Cambrian to Ordovician carbonate rocks and carried small xenoliths from the country rocks, especially the peridotite xenoliths in the dioritic rocks (Xu *et al.* 2010), implying that the melts were derived from the deep lithosphere and that the magma was emplaced rapidly. Meanwhile, the Sr–Nd isotopes of magmatic rocks in the Fushan pluton show nearly consistent $\varepsilon_{Nd}(t)$ values and slightly decreased Rb/Nb ratios with variable SiO_2 contents (Fig. 9a, b). These features suggest that the melt assimilation with the wall rock was insignificant before their emplacement.

The major elemental compositions of the samples show broad distributions and variations and decrease with the increasing SiO_2, including CaO, MgO, $Fe_2O_3^T$, TiO_2 and P_2O_5, while Al_2O_3 and Na_2O show the opposite trend (Fig. 5). These results indicate that the magmas of the Fushan pluton experienced a certain amount of fractional crystallization. The varied abundances and variations of the major and trace elements, e.g. MgO, Ni, Cr and the CaO/Al_2O_3 ratio, indicate the significant fractionation of ferromagnesian phases such as pyroxene (Fig. 10a, b). Meanwhile, the obvious fractional crystallization of amphibole is displayed by the variations in Ba and Sr and the Ba/Rb and Rb/Sr ratios (Fig. 1c, d), which are consistent with the presence of amphibole in the earlier phase of the rocks in the Fushan pluton but its absence in the rocks of the later phase. The separation of feldspar in the Fushan rocks appears minor, as suggested by the positive correlation between Al_2O_3 and SiO_2 (Fig. 10b) and positive Ba, Sr and Eu anomalies (Fig. 6). The fractionation of the minor and accessory minerals, e.g. titanite and apatite, is also shown by the related elemental variations in the TiO_2 and P_2O_5 contents (Fig. 5e, f). Thus, the above arguments suggest that the fractionation of ferromagnesian minerals, e.g. amphibole, was significant at the earlier stage of magma evolution in the magma chamber, while the feldspar removal was minor during the magma evolution process.

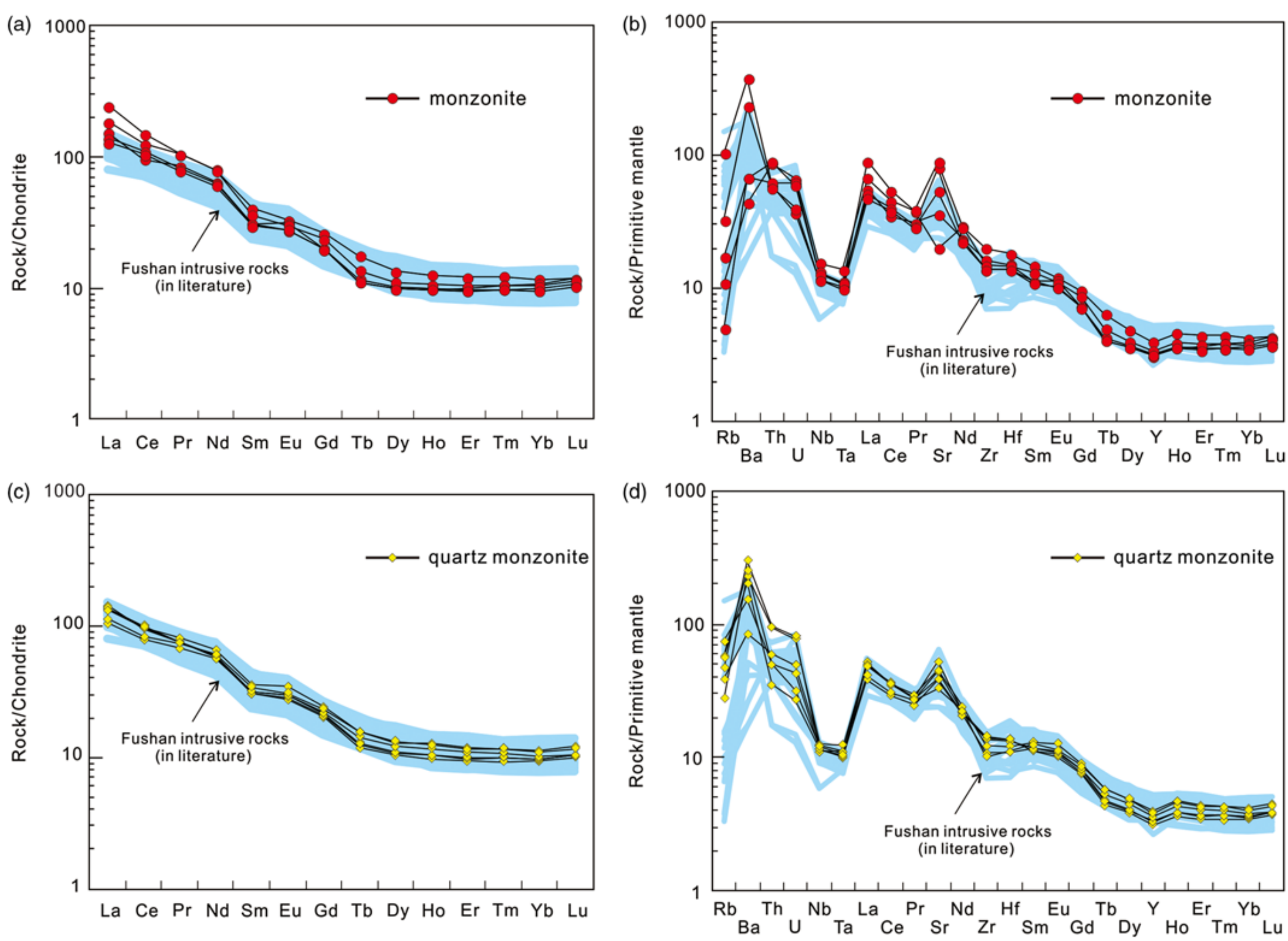

Fig. 6. (Colour online) (a) Chondrite-normalized REE patterns and (b) primitive mantle-normalized trace element diagrams for the monzonitic rocks in the Fushan pluton. Normalization values are from McDonough & Sun (1995).

https://doi.org/10.1017/S0016756819000256 Published online by Cambridge University Press

5.b.2. Source of magma

The monzonites and quartz monzonites have intermediate SiO_2 with relatively high mafic components, such as high $Fe_2O_3^T$, MgO, Cr and Ni contents with high Mg# values (Figs. 5a, b and 10a), implying that the parental magma was derived from the mantle, which is in accordance with previous studies (Chen *et al.* 2004; Xu *et al.* 2009b). The monzogabbros, monzonites and quartz monzonites from the Fushan pluton display nearly uniform Sr–Nd–Hf isotope components, suggesting they were not generated from a single juvenile lithospheric mantle or asthenospheric mantle (Huang *et al.* 2016).

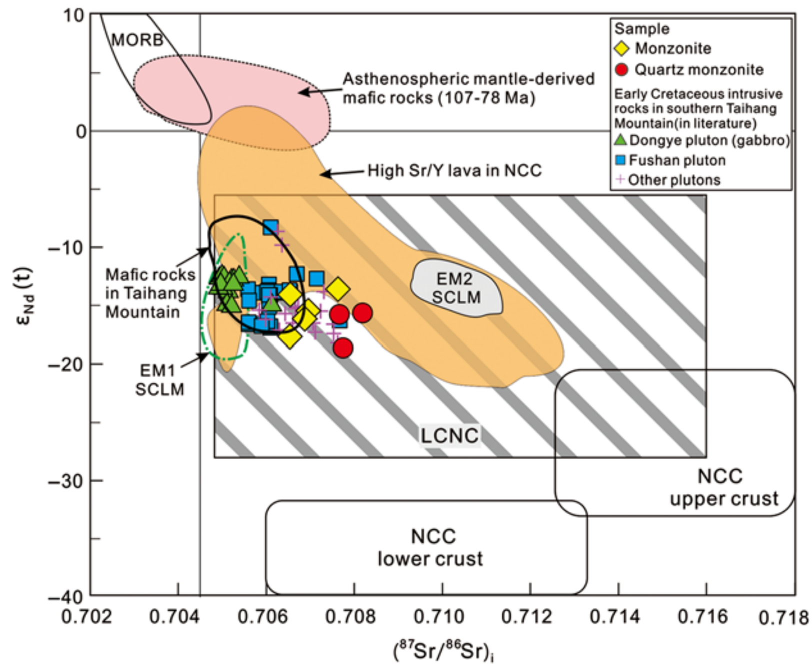

Fig. 7. (Colour online) Initial $^{87}Sr/^{86}Sr$ vs $\varepsilon_{Nd}(t)$ diagram. Data sources: Early Cretaceous intrusive rocks in the southern Taihang Mountains as shown in Figure 4; Late Mesozoic magmatic rocks in the NCC: high Sr/Y lava in the NCC (Ma *et al.* 2015); mafic rocks in the Taihang Mountains (Wang *et al.* 2006); asthenospheric mantle-derived mafic rocks (107–78 Ma) (Ma *et al.* 2014); EM1-SCLM and EM2-SCLM (Li *et al.* 2018 *c*); LCNC (lower crust of North China) (Jiang *et al.* 2013); NCC lower crust and NCC upper crust (Jahn *et al.* 1999).

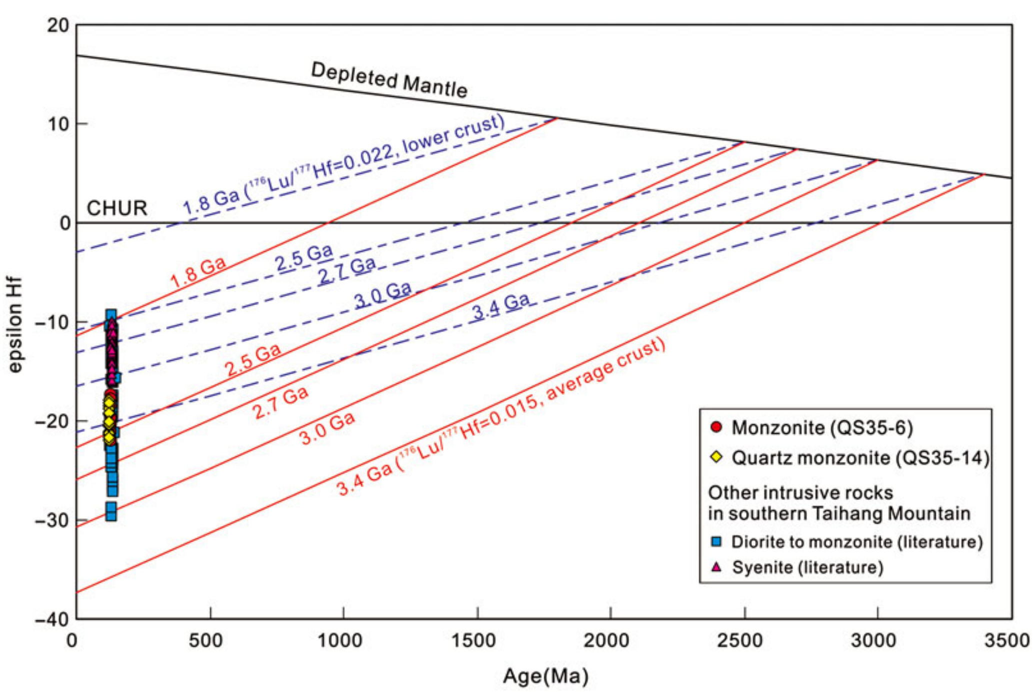

Fig. 8. (Colour online) Zircon $^{206}Pb/^{238}U$ ages vs $\varepsilon_{Hf}(t)$ diagram. Data sources for other intrusive rocks in the southern Taihang Mountains: diorite, monzonite, and syenite (Chen *et al.* 2008; Sun *et al.* 2014, 2015).

https://doi.org/10.1017/S0016756819000256 Published online by Cambridge University Press

They are all enriched in large ion lithophile elements (LILEs) and LREEs and depleted in high field strength elements (HFSEs); these features suggest that they could be derived from enriched lithospheric mantle similar to the EM-1 type enriched mantle (Fig. 7). A considerable amount of amphibole occurs in the monzonites, indicating that the parental magma of the monzonites included a quantity of water. Therefore, the enriched lithospheric mantle could have experienced fluid-related subduction metasomatism (Fig. 11b). The high Ba/Rb and low Rb/Sr ratios also imply the presence of amphibole in the mantle source of monzonites, rather than phlogopite (Furman & Graham, 1999) (Fig. 11c). In addition, the mantle metasomatism would considerably increase the concentrations of incompatible trace elements (e.g. Ba, Th, U, Sr and LREEs) in the mantle source by metasomatic agents, e.g. silicate melts, carbonate melts or C-H-O-rich fluids (Rudnick *et al.* 1993; Tarney and Jones, 1994; Blundy and Dalton, 2000). Compared with silicate metasomatism, carbonatitic metasomatism is often characterized by extreme LILE enrichment and obvious REE fractionation (Rudnick *et al.* 1993; Blundy and Dalton, 2000). Most samples show moderate LILE enrichment, and even depletion in Rb, and no HREE fractionation, which suggest silicate metasomatism rather than carbonatitic metasomatism. The samples show low Dy/Yb (1.6–1.9) and $(Gd/Yb)_N$ ratios (2.0–2.3) (Figs. 6, 11d), which suggest that they were mainly derived from spinel-facies mantle. The ancient Proterozoic isotopic model ages of the Fushan monzonites and quartz monzonites from Nd and Hf isotopes suggest that the enriched lithospheric mantle source could have been metasomatized by ancient subducted crustal materials. Therefore, the parental magma of the monzonites and quartz monzonites could mainly have been derived from the partial melting of a spinel-facies amphibole-bearing ancient (EM1-like) enriched lithospheric mantle source.

5.c. Genesis of high Ba–Sr and high Sr/Y signals

Previous studies have shown that other Early Cretaceous magmatic rocks in the Taihang Mountains also display high Ba–Sr or high Sr/Y signatures, and their genesis has been debated for a long time, with several suggestions such as the magma mixing of siliceous crustal melts and basaltic magma from metasomatized mantle (Chen *et al.* 2008, 2013; Wang *et al.* 2017), partial melting of the delaminated lower crust interacting with mantle peridotite (Xu *et al.* 2010), partial melting of the ancient lower continental crust emphasizing source inheritance (Qian & Hermann, 2010) or efficient magmatic processes of crystal fractionation (Gao *et al.* 2012). In this study, the Fushan monzonites and quartz monzonites exhibit two important geochemical features: high Ba–Sr and high Sr/Y signatures. They display the geochemical features of high Ba (289–2454 ppm) and Sr (395–1756 ppm), similar to the defined high Ba–Sr intrusions (Ba and Sr in excess of 1000 ppm) (Fig. 1c), high alkali elements and varying MgO (<16 wt %) and SiO_2 (>47 wt %) contents (Fowler *et al.* 2001). Most of the samples also have high Sr/Y (>20) signatures with high Sr (>350 ppm), low Y (<17 ppm) and Yb (<1.8 ppm) contents, and a lack of obvious Eu anomalies, similar to adakitic rocks (Drummond & Defant, 1990; Martin *et al.* 2005; Castillo, 2012) (Fig. 12). Firstly, the samples show some geochemical features different from those of typical adakitic rocks in modern subduction zones, which have higher La/Yb ratios and depleted Sr–Nd isotopes (Castillo, 2012). Additionally, the adakitic rocks, formed by the partial melting of a thickened/delaminated lower crust, usually have an obvious depletion and high differentiation in HREEs related to garnet in the restites, while these samples mainly show flat HREE patterns without obvious differentiation in HREEs (Figs. 6a, b and 10f) and are mainly derived from an enriched subcontinental lithospheric mantle (SCLM) source, which could not

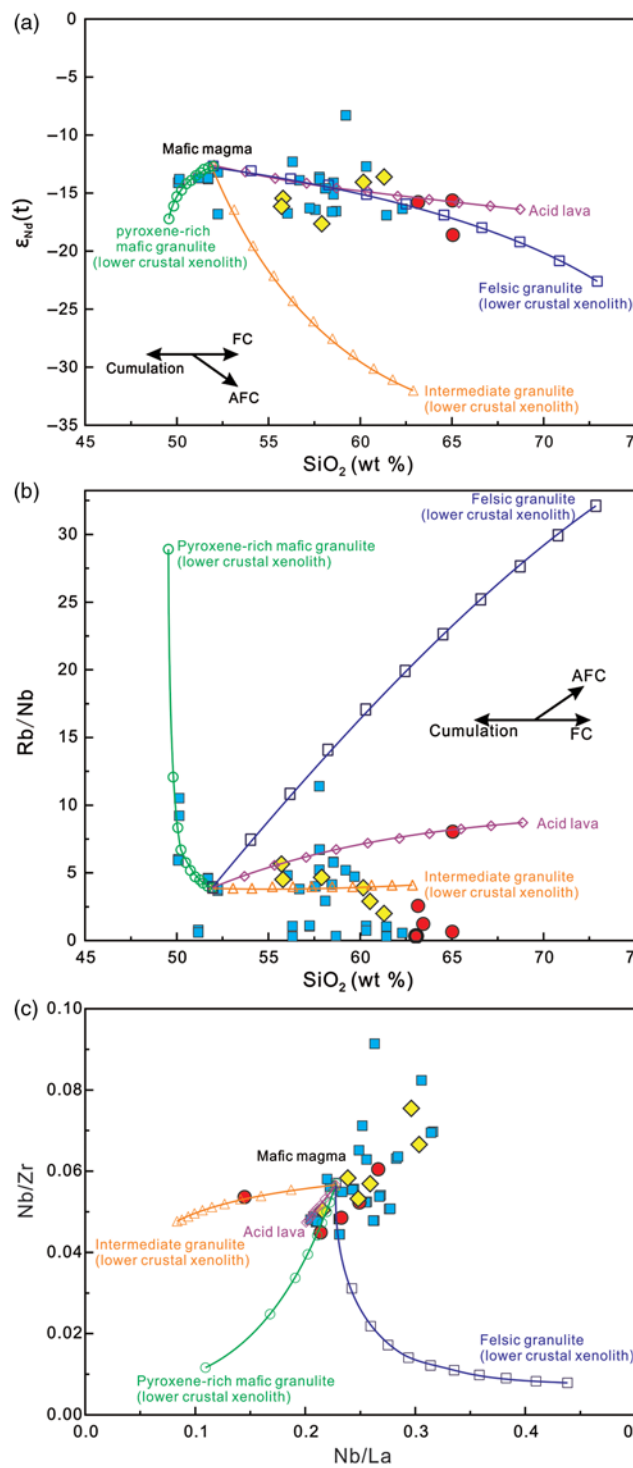

Fig. 9. (Colour online) (a) SiO_2 vs $\varepsilon_{Nd}(t)$, (b) SiO_2 vs Rb/Nb and (c) Nb/La vs Nb/Zr diagrams. Data sources: Early Cretaceous intrusive rocks in the southern Taihang Mountains as shown in Figure 4. End-members used in the mixing model: mafic magma (sample 20HD-78 in Wang *et al.* 2006); acid lava (sample LMT-3 in Gao *et al.* 2012); lower crustal xenoliths from the central NCC: pyroxene-rich mafic granulite (JN0918 in Jiang *et al.* 2011), intermediate granulite (JN0811 in Jiang *et al.* 2011) and felsic granulite (ZB-20 in Liu *et al.* 2001, 2004).

https://doi.org/10.1017/S0016756819000256 Published online by Cambridge University Press

involve many thickened/delaminated lower crustal components. Previous studies have shown that the magma mixing of crust- and mantle-derived magmas played an important role in the genesis of the Early Cretaceous magmatic rocks in the NCC (Chen *et al.* 2008, 2013). The mantle-derived magmatic rocks were developed in the central and eastern NCC during the Early Cretaceous, e.g. mafic dykes and intrusions (Wang *et al.* 2006). These rocks imply that the magmatic underplating influenced the deep crust beneath the central NCC (Zhai *et al.* 2007). In addition, the deep crustal xenoliths carried by Cenozoic basalts in the NCC are usually dated to ~160–140 Ma (Liu *et al.* 2001, 2004; Jiang *et al.* 2013). These crustal xenoliths are considered as products of basaltic magmatic underplating into the lower crust during the late Mesozoic (Late Jurassic to Cretaceous), which then experienced the fractional crystallization of a magma chamber in the lower crust (Liu *et al.* 2004). These mafic, intermediate and felsic granulite crustal xenoliths are used to represent the components of the lower to middle crust beneath the central NCC (Liu *et al.* 2001). The mixing of two end-members was modelled by the Early Cretaceous mantle-derived gabbro in the southern Taihang Mountains with different crustal xenoliths or volcanic rocks. The model results show that the elemental and isotopic features of the Fushan monzonites and quartz monzonites are not simply modelled by a mantle-derived magma mixed with a Cretaceous felsic or intermediate magma (Fig. 9a, b, c).

Even though the magma mixing model is required in their genesis, at least one of two other factors is needed to explain the high Ba–Sr and high Sr/Y signatures; one factor is that either crust- or mantle-derived magmas inherited these signatures from their sources, and the other factor is that magmatic processes such as crystal fractionation induced these features. The high Ba–Sr intrusions usually have varied rock types from appinite to granite with evolution from mafic to intermediate-acid rocks (Fowler *et al.* 2001; Ye *et al.* 2008). Their high Ba–Sr features are usually inherited from the source, while the contents of Ba and Sr are obviously influenced by magmatic evolution, e.g. fractional crystallization (Fowler *et al.* 2001, 2008). The end-members of the mafic magma for the Fushan pluton are the monzogabbros (Chen *et al.* 2004; Xu *et al.* 2009b). The above arguments suggest that the fractionation of ferromagnesian minerals was significant during the earlier stage of magma evolution in the magma chamber, while the feldspar removal was minor. Thus, the monzonites are cogenetic with the monzogabbros and could be the products of a later stage in the magmatic evolution from mafic to intermediate rocks. The Fushan monzogabbros have lower SiO_2 and higher MgO and Fe_2O_3 contents than the monzonites, with high Sr (569–732 ppm) and Ba (116–907 ppm) contents (Chen *et al.* 2004). Meanwhile, some contemporaneous gabbros occur near the Fushan pluton in the southern Taihang Mountains. For example, the Cretaceous (125 Ma) Dongye gabbro intrusions show features similar to those of the monzogabbros in their Sr (444–758 ppm) and Ba (409–899 ppm) values (Wang *et al.* 2006). However, the Fushan monzonite samples have higher Sr (395–1756 ppm) and Ba (289–1997 ppm) than the monzogabbros and gabbro intrusions (Fig. 8e).

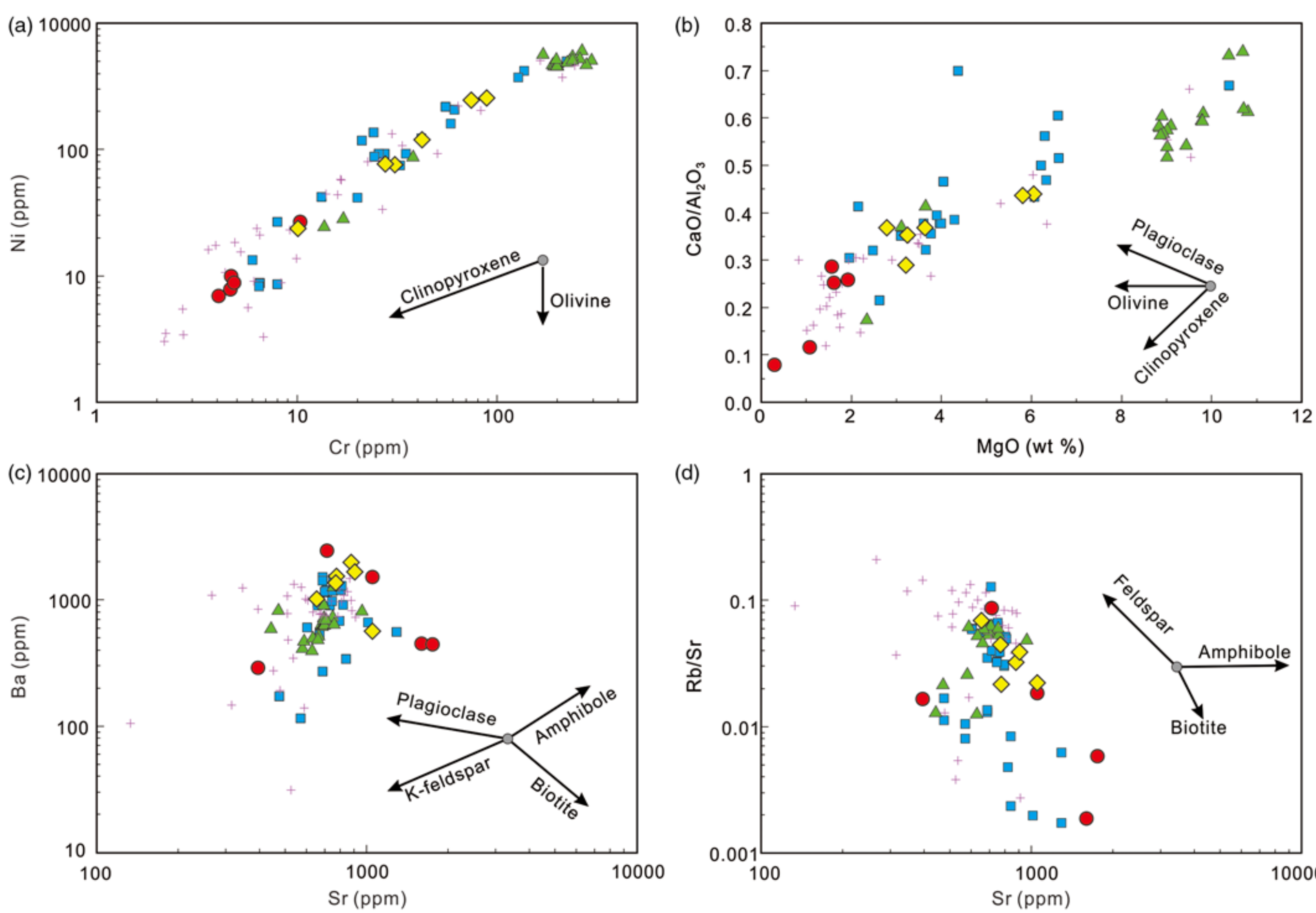

Fig. 10. (Colour online) Element variations of (a) CaO/Al_2O_3 vs MgO; (b) Cr vs Ni; (c) Ba vs Sr; and (d) Rb/Sr vs Sr. Data sources as shown in Figure 4.

https://doi.org/10.1017/S0016756819000256 Published online by Cambridge University Press

The fractional crystallization of amphibole could lead to obvious increases in the Ba and Sr concentrations, and the fractionation of feldspar would result in an obvious Sr decrease and varying Ba concentrations. The Fushan pluton indicates the fractional crystallization of amphibole and some feldspar from monzonites to quartz monzonites with increased Sr and Ba (Fig. 1c, d). Then, on the basis of the high Ba–Sr features inherited from the magmatic source, the high Ba–Sr contents could also reflect a great contribution by fractional crystallization.

The Fushan monzonite samples have low Yb (1.5–1.8 ppm) and Y (13–17 ppm) contents with high Sr/Y ratios (23–121). The Fushan monzogabbros and Dongye gabbro intrusions have similar low Yb (1.0–2.2 ppm) and Y (12–20 ppm) contents but lower Sr/Y ratios (28–57) (Wang *et al.* 2006; Chen *et al.* 2008). It is necessary to note that the monzogabbros with low SiO_2 contents in the Fushan pluton also show geochemical features of adakitic rocks, with similarly low Yb and Y contents but lower Sr/Y ratios than the monzonites. These results imply that the geochemical features of the Fushan pluton, especially the low Yb and Y, are inherited from their original magma chamber or magma source. In addition, the Sr/Y ratios increase from the monzogabbros to monzonites, which could be related to the increased Sr contents with similar Y and Yb contents. As mentioned above, the Fushan pluton could have experienced a significant process of crystal fractionation from mafic to intermediate rocks, which may have facilitated the increase in the Sr content. The study of the genesis of adakitic rocks shows that the fractionation of hornblende usually induces higher Sr/Y ratios with increased Sr contents. In addition, the modelled partial melting curves show that the Fushan intrusive rocks are different because they are simply explained by the partial melting trends and the mafic lower crust of the NCC with different restites, which usually require a large degree of partial melting (Ma *et al.* 2015) (Fig. 12a) and a normal mid-ocean ridge basalt (N-MORB) bulk composition (Castillo, 2012) (Fig. 12c). Meanwhile, the modelled Rayleigh fractionation of hornblende can usually induce such Sr/Y and La/Y ratios (Fig. 12b, d). Therefore, the geochemical features of the Fushan intrusive rocks, e.g. high Ba–Sr concentrations and high Sr/Y ratios, are not only inherited from the magma source but also significantly enhanced by crystal fractionation during the magmatic evolution, e.g. the hornblende fractionation increased the Ba–Sr concentrations and Sr/Y ratios.

5.d. Tectonic implications

The destruction of the eastern NCC is mainly revealed by investigations of the magmatism and peridotite xenoliths, suggesting that a relatively cold, thick and refractory cratonic lithospheric mantle during the Palaeozoic was replaced by a hot, thin and fertile mantle during the Meso-Cenozoic (Gao *et al.* 2004; Wu *et al.* 2006; Zheng *et al.* 2006; Zhang, 2009; Zheng, 2009). The major hypotheses for

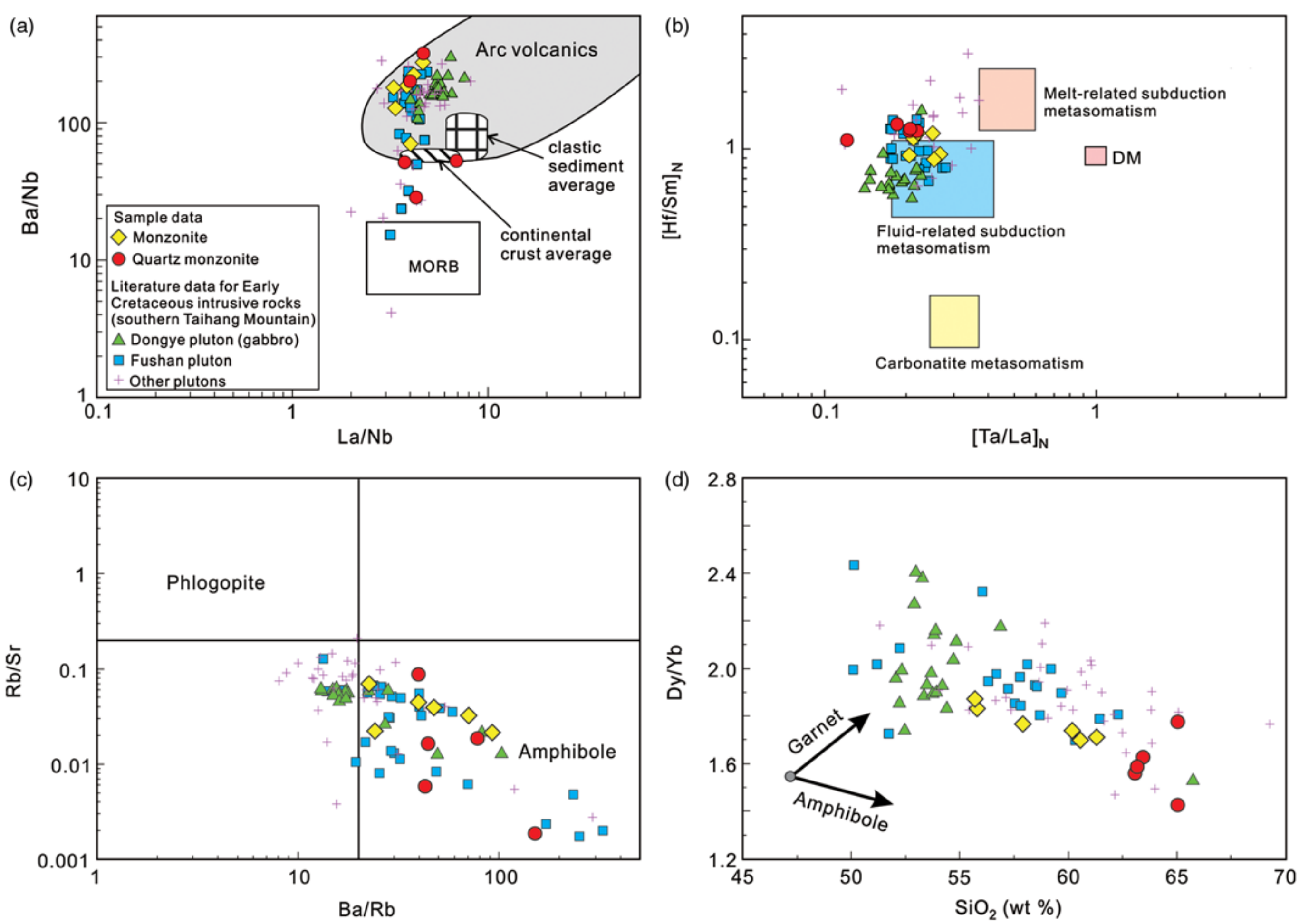

Fig. 11. (Colour online) Diagrams of (a) La/Nb vs Ba/Nb (after Jahn *et al.* 1999); (b) $[Ta/La]_N$ vs $[Hf/Sm]_N$ (after La Fleche *et al.* 1998). N stands for primitive mantle-normalized. (c) Rb/Sr vs Ba/Rb; (d) SiO_2 vs Dy/Yb (after Davidson *et al.* 2007). Data sources as shown in Figure 4.

https://doi.org/10.1017/S0016756819000256 Published online by Cambridge University Press

this mechanism of destruction of the eastern NCC include the thermal–tectonic erosion of the Archaean lithospheric keel (Xu *et al.* 2009a; Zheng, 2009), a peridotite–melt reaction to transform the lithospheric mantle (Zhang, 2009), the delamination of thickened lower continental crust and lithospheric mantle (Gao *et al.* 2004; Xu *et al.* 2013) and the multiple subduction and water addition events (Niu, 2005; Windley *et al.* 2010). Some studies have argued for a lithospheric gravitational instability process that may explain the mechanism for the coexistence of ancient and juvenile lithospheric mantle components within the present-day NCC lithosphere (Wang *et al.* 2015, 2016*b*). More importantly, the subduction of the Palaeo-Pacific Plate has received increasing recognition of its key role in the geodynamic processes beneath the East Asia continent, including the eastern NCC (Zhu *et al.* 2012; Zheng *et al.* 2018).

The Early Cretaceous is considered as the major period for the destruction of the eastern NCC, which was accompanied by intense magmatism and mineralization (Xu *et al.* 2009a; Zhu *et al.* 2012). The Cretaceous magmatism not only happened on the margin of the NCC but also produced a series of mafic to intermediate intrusions in the central NCC, including the Fushan pluton (Li, 2013; Zhang *et al.* 2014). There are also some metamorphic core complexes (Liu *et al.* 2013), extensional basins (Li *et al.* 2012*b*), and gold and iron deposits (Li *et al.* 2012*a*; Deng *et al.* 2015) that are coeval with the large-scale Early Cretaceous magmatism in the eastern and central NCC. These features imply that the eastern and central NCC were under a lithospheric extensional setting during the Early Cretaceous. Compared with the eastern NCC, the southern Taihang Mountains of the central NCC were mainly in an intracontinental setting during the late Mesozoic and could have experienced the Late Triassic – Late Jurassic and Late Jurassic – Early Cretaceous intracontinental orogenic processes inherited from the pre-existing thrust tectonics developed at an Early to Middle Triassic comprehensive collisional stage (Li *et al.* 2015). Meanwhile, the lithosphere beneath the central NCC could be complex, with the coexistence of ancient and newly accreted mantle and crustal components (Zheng *et al.* 2001; Tang *et al.* 2013; Zhang *et al.* 2013). These juvenile crustal and mantle materials could be related to asthenospheric upwelling and magmatic underplating under a lithospheric extensional setting (Zhai *et al.* 2007; Tang *et al.* 2013; Zhang *et al.* 2013). Thus, these tectonic and magmatic events imply that the central NCC was under lithospheric extension in an intracontinental setting in the Early Cretaceous.

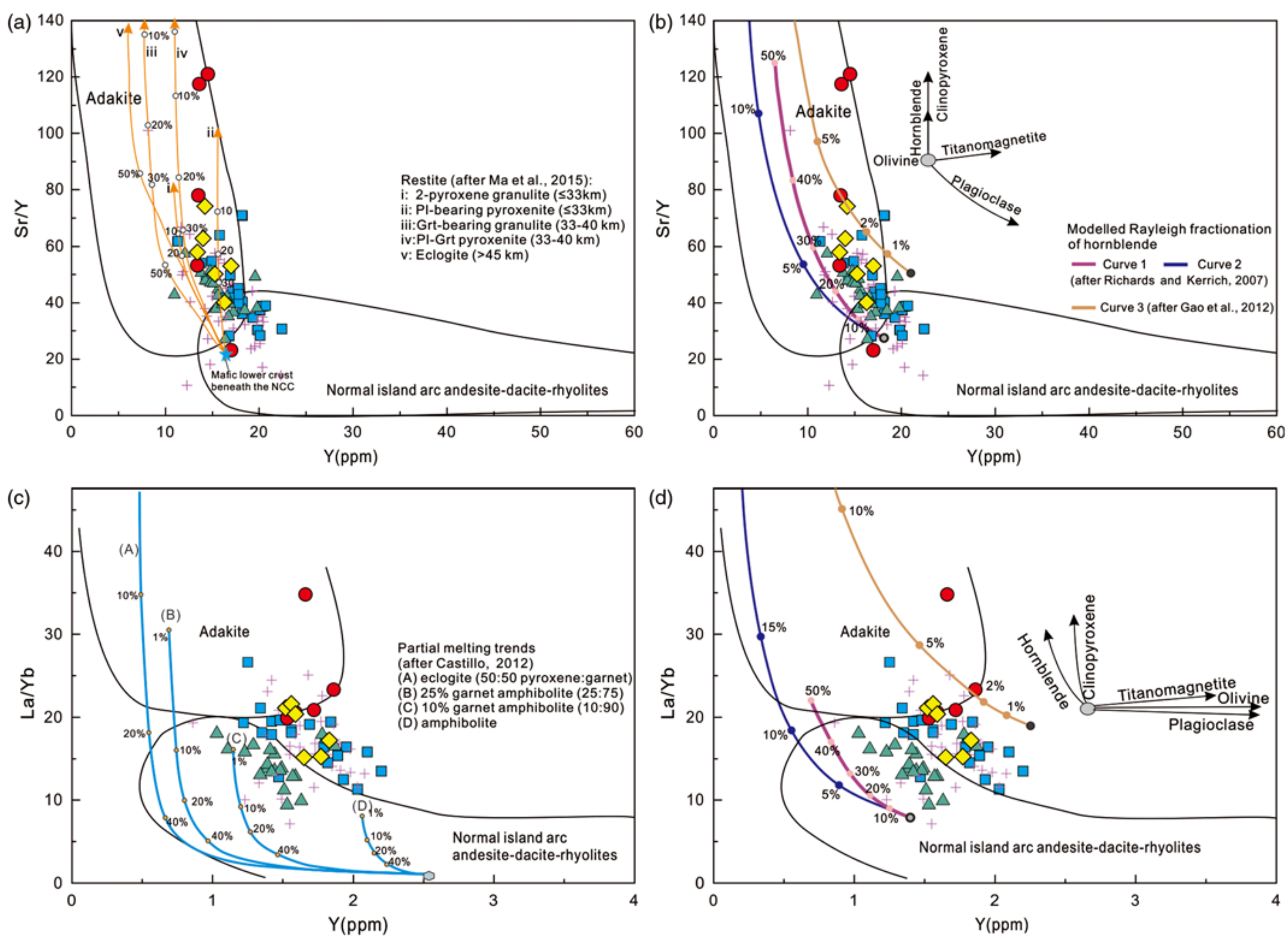

Fig. 12. (Colour online) (a, b) Sr/Y vs Y (after Drummond & Defant, 1990; Ma *et al.* 2015); (c, d) La/Yb vs Yb (after Castillo, 2012) diagrams. (a) Partial melting curves calculated for the mafic lower crust of the NCC with different restites after Ma *et al.* (2015). (c) partial melting trends of (a) eclogite (50:50 pyroxene: garnet), (b) 25 % garnet amphibolite (25:75), (c) 10 % garnet amphibolite (10:90) and (d) amphibolite, all with a starting N-MORB bulk composition after Castillo (2012). (b, d) Modelled Rayleigh fractionation of hornblende: curves 1 and 2 after Richards & Kerrich (2007) and curve 3 after Gao *et al.* (2012).

https://doi.org/10.1017/S0016756819000256 Published online by Cambridge University Press

Studies of plate reconstructions show the Mesozoic geodynamic process of Palaeo-Pacific subduction beneath the East Asia continent, and the age of the subducting slab of the Palaeo-Pacific Plate gradually became younger (Seton *et al.* 2012; Müller *et al.* 2016). According to the width of the present subduction zone, the mantle wedge beneath the arc system seems to be unable to have extended to the central NCC (Maruyama *et al.* 2009). Meanwhile, the present geophysical and seismic tomography display the stagnation of the Pacific Plate in the mantle transition zone beneath the East Asia continental margin and the formation of a big mantle wedge (Huang & Zhao, 2006; Zhao *et al.* 2007; Liu *et al.* 2017). Some geochemical studies have suggested that the Mesozoic process could have been similar to the current subduction of the Pacific Plate beneath East Asia, forming a stagnant slab that extended down to the mantle transition zone (Li & Wang, 2018; Xu *et al.* 2018). Recently, reconstructions of the time-dependent dynamic topography of Eastern China have indicated that the slab of the Palaeo-Pacific Plate subducted into the deeper section of the upper mantle beneath East Asia during the Early Cretaceous (Cao *et al.* 2018). Meanwhile, the sinking and roll-back of the Palaeo-Pacific slab happened from the late Early Cretaceous to Late Cretaceous (Cao *et al.* 2018). In addition, the lithospheric extensional setting of the eastern NCC during the late Mesozoic is suggested to be related to the possible slab roll-back of the Pacific Plate (Yang *et al.* 2010; Li *et al.* 2018*c*). Accordingly, the lithospheric extensional setting under the central NCC could have been related to the sinking and roll-back of the Palaeo-Pacific slab. Then, the slab sinking and roll-back of the Palaeo-Pacific Plate could have created an ancient big mantle wedge beneath East Asia and induced a lithospheric extensional process in the central NCC within an intracontinental setting during the Early Cretaceous.

6. Conclusions

A comprehensive geochronological, geochemical and Sr–Nd–Hf isotopic study of the monzonites and quartz monzonites from the Fushan pluton in the southern Taihang Mountains, central NCC, has led to the following conclusions: (1) zircon U–Pb dating results indicate that the Fushan pluton was emplaced during 126–124 Ma; (2) the primary magma of the Fushan pluton was a product of the partial melting of spinel-facies amphibole-bearing ancient (EM1-like) enriched lithospheric mantle; (3) the particular geochemical features of the Fushan pluton, e.g. high Ba–Sr and low Y and Yb contents with high Sr/Y ratios, are not only inherited from the magma source but also significantly enhanced by crystal fractionation during magmatic evolution, e.g. hornblende fractionation increased the Ba–Sr concentrations and Sr/Y ratios; and (4) the Fushan pluton was formed by lithospheric extension in an intracontinental setting in the central NCC during the Early Cretaceous, which was related to the slab sinking and roll-back of the Palaeo-Pacific Plate beneath East Asia.

Supplementary material. To view supplementary material for this article, please visit https://doi.org/10.1017/S0016756819000256.

Author ORCIDs. Xi-Yao Li, 0000-0001-9750-5408; San-Zhong Li 0000-0002-3436-2793

Acknowledgements. We thank Dr. Deering Chad and two anonymous referees for their valuable comments. This research was funded by the National Science and Technology Major Project (grant number 2016ZX05004001); the National Key Research and Development Program of China (grant numbers 2017YFC0601401, 2016YFC0601002); the National Natural Science Foundation of China (grant numbers 41602042, U1606401); and the Scientific and Technological Innovation Project (grant number 2016ASKJ13) of Qingdao National Laboratory for Marine Science and Technology. This work was also supported by the Taishan Scholar Program to Prof. San-Zhong Li.

References

Amelin Y, Lee DC, Halliday AN and Pidgeon RT (1999) Nature of the Earth's earliest crust from hafnium isotopes in single detrital zircons. *Nature* **399**, 252.

Annen C, Blundy JD and Sparks RSJ (2005) The genesis of intermediate and silicic magmas in deep crustal hot zones. *Journal of Petrology* **47**, 505–39.

Blundy J and Dalton J (2000) Experimental comparison of trace element partitioning between clinopyroxene and melt in carbonate and silicate systems, and implications for mantle metasomatism. *Contributions to Mineralogy and Petrology* **139**, 356–71.

Bouvier A, Vervoort JD and Patchett PJ (2008) The Lu–Hf and Sm–Nd isotopic composition of CHUR: constraints from unequilibrated chondrites and implications for the bulk composition of terrestrial planets. *Earth and Planetary Science Letters* **273**, 48–57.

Bruand E, Storey C and Fowler M (2014) Accessory mineral chemistry of high Ba–Sr granites from Northern Scotland: constraints on petrogenesis and records of whole-rock signature. *Journal of Petrology* **55**, 1619–51.

Cao XZ, Flament N, Müller D and Li SZ (2018) The dynamic topography of Eastern China since the latest Jurassic Period. *Tectonics* **37**, 1274–91.

Castillo PR (2012) Adakite petrogenesis. *Lithos* **134–135**, 304–16.

Chen B, Chen ZC and Jahn BM (2009) Origin of mafic enclaves from the Taihang Mesozoic orogen, north China craton. *Lithos* **110**, 343–58.

Chen B, Jahn BM, Arakawa Y and Zhai MG (2004) Petrogenesis of the Mesozoic intrusive complexes from the southern Taihang Orogen, North China Craton: elemental and Sr–Nd–Pb isotopic constraints. *Contributions to Mineralogy and Petrology* **148**, 489–501.

Chen B, Jahn BM and Suzuki K (2013) Petrological and Nd-Sr-Os isotopic constraints on the origin of high-Mg adakitic rocks from the North China Craton: tectonic implications. *Geology* **41**, 91–4.

Chen B, Tian W, Jahn BM and Chen ZC (2008) Zircon SHRIMP U–Pb ages and in-situ Hf isotopic analysis for the Mesozoic intrusions in South Taihang, North China craton: evidence for hybridization between mantle-derived magmas and crustal components. *Lithos* **102**, 118–37.

Chen FK, Satir M, Ji J and Zhong D (2002) Nd–Sr–Pb isotopes of Tengchong Cenozoic volcanic rocks from western Yunnan, China: evidence for an enriched-mantle source. *Journal of Asian Earth Sciences* **21**, 39–45.

Davidson J, Turner S, Handley H, MacPherson C and Dosseto A (2007) Amphibole "sponge" in arc crust? *Geology* **35**, 787.

Deng XD, Li JW and Wen G (2015) U-Pb geochronology of hydrothermal zircons from the Early Cretaceous iron skarn deposits in the Handan-Xingtai District, North China Craton. *Economic Geology* **110**, 2159–80.

Depaolo DJ (1981) Trace element and isotopic effects of combined wallrock assimilation and fractional crystallization. *Earth and Planetary Science Letters* **53**, 189–202.

Dong JH, Chen B and Zhou L (2003) Petrogenesis of the Fushan pluton from the south Taihang Mountain: evidence from petrology and geochemistry. *Progress in Natural Science* **7**, 97–104 (in Chinese with English abstract).

Drummond MS and Defant MJ (1990) A model for Trondhjemite-Tonalite-Dacite Genesis and crustal growth via slab melting: Archean to modern comparisons. *Journal of Geophysical Research: Solid Earth* **95**, 21503–21.

Foley SF, Tiepolo M and Vannucci R (2002) Growth of early continental crust controlled by melting of amphibolite in subduction zones. *Nature* **417**, 837–40.

Fowler MB, Henney PJ, Darbyshire DPF and Greenwood PB (2001) Petrogenesis of high Ba-Sr granites: the Rogart pluton, Sutherland. *Journal of the Geological Society* **158**, 521–34.

Fowler MB, Kocks H, Darbyshire DPF and Greenwood PB (2008) Petrogenesis of high Ba–Sr plutons from the Northern Highlands Terrane of the British Caledonian Province. *Lithos* **105**, 129–48.

Frost BR, Barnes CG, Collins WJ, Arculus RJ, Ellis DJ and Frost CD (2001) A geochemical classification for granitic rocks. *Journal of Petrology* **42**, 2033–48.

Furman T and Graham D (1999) Erosion of lithospheric mantle beneath the East African Rift system: geochemical evidence from the Kivu volcanic province. *Developments in Geotectonics* **24**, 237–62.

Gao S, Rudnick RL, Yuan HL, Liu XM, Liu YS, Xu WL, Ling WL, Ayers J, Wang XC and Wang QH (2004) Recycling lower continental crust in the North China craton. *Nature* **432**, 892–7.

Gao YF, Santosh M, Hou ZQ, Wei RH, Ma GX, Chen ZK and Wu JL (2012) High Sr/Y magmas generated through crystal fractionation: evidence from Mesozoic volcanic rocks in the northern Taihang orogen, North China Craton. *Gondwana Research* **22**, 152–68.

Gao YF, Santosh M, Wei RH, Ma GX, Chen ZK and Wu JL (2013) Origin of high Sr/Y magmas from the northern Taihang Mountains: implications for Mesozoic porphyry copper mineralization in the North China Craton. *Journal of Asian Earth Sciences* **78**, 143–59.

Griffin WL, Wang X, Jackson SE, Pearson NJ, O'Reilly SY, Xu X and Zhou X (2002) Zircon chemistry and magma mixing, SE China: in-situ analysis of Hf isotopes, Tonglu and Pingtan igneous complexes. *Lithos* **61**, 237–69.

Huang F, Xu JF, Chen JL, Wu JB, Zeng YC, Xiong QW, Chen XF and Yu HX (2016) Two Cenozoic tectonic events of N–S and E–W extension in the Lhasa Terrane: evidence from geology and geochronology. *Lithos* **245**, 118–32.

Huang F, Xu JF, Liu YS, Li J, Chen JL and Li XY (2017) Re–Os isotope evidence from Mesozoic and Cenozoic basalts for secular evolution of the mantle beneath the North China Craton. *Contributions to Mineralogy and Petrology* **172**, 28.

Huang JL and Zhao DP (2006) High-resolution mantle tomography of China and surrounding regions. *Journal of Geophysical Research: Solid Earth* **111**, 4813–25.

Jahn BM, Wu FY, Lo CH and Tsai CH (1999) Crust-mantle interaction induced by deep subduction of the continental crust: geochemical and Sr-Nd isotopic evidence from post-collisional mafic-ultramafic intrusions of the northern Dabie complex, central China. *Chemical Geology* **157**, 119–46.

Jiang N, Carlson RW and Guo J (2011) Source of Mesozoic intermediate-felsic igneous rocks in the North China craton: granulite xenolith evidence. *Lithos* **125**, 335–46.

Jiang N, Guo JH and Chang GH (2013) Nature and evolution of the lower crust in the eastern North China craton: a review. *Earth-Science Reviews* **122**, 1–9.

La Fleche MR, Camire G and Jenner GA (1998) Geochemistry of post-Acadian, Carboniferous continental intraplate basalts from the Maritimes Basin, Magdalen islands, Quebec, Canada. *Chemical Geology* **148**, 115–36.

Le Maitre RW (2002) *Igneous Rocks: A Classification and Glossary of Terms*, 2nd ed. Cambridge: Cambridge University Press, 236 pp.

Li HY (2013) Destruction of North China Craton: insights from temporal and spatial evolution of the proto-basins and magmatism. *Science China Earth Sciences* **56**, 464–78.

Li JW, Bi SJ, Selby D, Chen L, Vasconcelos P, Thiede D, Zhou MF, Zhao XF, Li ZK and Qiu HN (2012*a*) Giant Mesozoic gold provinces related to the destruction of the North China craton. *Earth and Planetary Science Letters* **349–350**, 26–37.

Li Q, Santosh M, Li SR and Guo P (2014) The formation and rejuvenation of continental crust in the central North China Craton: evidence from zircon U–Pb geochronology and Hf isotope. *Journal of Asian Earth Sciences* **95**, 17–32.

Li SG and Wang Y (2018) Formation time of the big mantle wedge beneath eastern China and a new lithospheric thinning mechanism of the North China craton: geodynamic effects of deep recycled carbon. *Science China Earth Sciences* **61**, 853.

Li SZ, Guo LL, Xu LQ, Somerville ID, Cao XZ, Yu S, Wang PC, Suo YH, Liu X and Zhao SJ (2015) Coupling and transition of Meso–Cenozoic intracontinental deformation between the Taihang and Qinling Mountains. *Journal of Asian Earth Sciences* **114**, 188–202.

Li SZ, Zhao GC, Dai LM, Liu X, Zhou LH, Santosh M and Suo YH (2012*b*) Mesozoic basins in eastern China and their bearing on the deconstruction of the North China Craton. *Journal of Asian Earth Sciences* **47**, 64–79.

Li SZ, Zhao SJ, Liu X, Cao HH, Yu S, Li XY, Somerville I, Yu SY and Suo YH (2018*a*) Closure of the Proto-Tethys Ocean and Early Paleozoic amalgamation of microcontinental blocks in East Asia. *Earth-Science Reviews* **186**, 37–75.

Li XY, Li SZ, Suo YH, Dai LM, Guo LL, Ge FJ and Lin PJ (2018*b*) Late Cretaceous basalts and rhyolites from Shimaoshan Group in eastern Fujian Province, SE China: age, petrogenesis, and tectonic implications. *International Geology Review* **60**, 1721–43.

Li XY, Li SZ, Suo YH, Somerville ID, Huang F, Liu X, Wang PC, Han ZX and Jin LJ (2018*c*) Early Cretaceous diabases, lamprophyres and andesites-dacites in western Shandong, North China Craton: implications for local delamination and Paleo-Pacific slab rollback. *Journal of Asian Earth Sciences* **160**, 426–44.

Liu JL, Shen L, Ji M, Guan HM, Zhang ZC and Zhao ZD (2013) The Liaonan/Wanfu metamorphic core complexes in the Liaodong Peninsula: two stages of exhumation and constraints on the destruction of the North China Craton. *Tectonics* **32**, 1121–41.

Liu SA, Li SG, Guo SS, Hou ZH and He YS (2012) The Cretaceous adakitic–basaltic–granitic magma sequence on south-eastern margin of the North China Craton: implications for lithospheric thinning mechanism. *Lithos* **134–135**, 163–78.

Liu X, Zhao DP, Li SZ and Wei W (2017) Age of the subducting Pacific slab beneath East Asia and its geodynamic implications. *Earth and Planetary Science Letters* **464**, 166–74.

Liu YS, Gao S, Hu ZC, Gao CG, Zong KQ and Wang DB (2010) Continental and oceanic crust recycling-induced melt-peridotite interactions in the Trans-North China Orogen: U–Pb dating, Hf isotopes and trace elements in zircons from mantle xenoliths. *Journal of Petrology* **51**, 537–71.

Liu YS, Gao S, Jin SY, Hu SH, Sun M, Zhao ZB and Feng JL (2001) Geochemistry of lower crustal xenoliths from Neogene Hannuoba Basalt, North China Craton: implications for petrogenesis and lower crustal composition. *Geochimica et Cosmochimica Acta* **65**, 2589–604.

Liu YS, Gao S, Yuan HL, Zhou L, Liu XM, Wang XC, Hu ZC and Wang LS (2004) U–Pb zircon ages and Nd, Sr, and Pb isotopes of lower crustal xenoliths from North China Craton: insights on evolution of lower continental crust. *Chemical Geology* **211**, 87–109.

Ma L, Jiang S, Hofmann AW, Dai B, Hou M, Zhao K, Chen L, Li J and Jiang Y (2014) Lithospheric and asthenospheric sources of lamprophyres in the Jiaodong Peninsula: a consequence of rapid lithospheric thinning beneath the North China Craton? *Geochimica et Cosmochimica Acta* **124**, 250–71.

Ma Q, Xu YG, Zheng JP, Griffin WL, Hong LB and Ma L (2016*a*) Coexisting Early Cretaceous high-Mg andesites and adakitic rocks in the North China Craton: the role of water in intraplate magmatism and cratonic destruction. *Journal of Petrology* **57**, 1279–308.

Ma Q, Xu YG, Zheng JP, Sun M, Griffin WL, Wei Y, Ma L and Yu XL (2016*b*) High-Mg adakitic rocks and their complementary cumulates formed by crystal fractionation of hydrous mafic magmas in a continental crustal magma chamber. *Lithos* **260**, 211–24.

Ma Q, Zheng J, Xu Y, Griffin WL and Zhang R (2015) Are continental "adakites" derived from thickened or foundered lower crust? *Earth and Planetary Science Letters* **419**, 125–33.

Maniar PD and Piccoli PM (1989) Tectonic discrimination of granitoids. *Geological Society of America Bulletin* **101**, 635–43.

Martin H, Smithies RH, Rapp R, Moyen JF and Champion D (2005) An overview of adakite, tonalite–trondhjemite–granodiorite (TTG), and sanukitoid: relationships and some implications for crustal evolution. *Lithos* **79**, 1–24.

Maruyama S, Hasegawa A, Santosh M, Kogiso T, Omori S, Nakamura H, Kawai K and Zhao D (2009) The dynamics of big mantle wedge, magma factory, and metamorphic–metasomatic factory in subduction zones. *Gondwana Research* **16**, 414–30.

McDonough WF and Sun SS (1995) The composition of the Earth. *Chemical Geology* **120**, 223–53.

Morel MLA, Nebel O, Nebel-Jacobsen YJ, Miller JS and Vroon PZ (2008) Hafnium isotope characterization of the GJ-1 zircon reference material by solution and laser-ablation MC-ICPMS. *Chemical Geology* **255**, 231–5.

Müller RD, Seton M, Zahirovic S, Williams SE, Matthews KJ, Wright NM, Shephard GE, Maloney KT, Barnettmoore N and Hosseinpour M (2016) Ocean basin evolution and global-scale plate reorganization events since Pangea breakup. *Annual Review of Earth & Planetary Sciences* **44**, 107–38.

Niu YL (2005) Generation and evolution of basaltic magmas: some basic concepts and a new view on the origin of Mesozoic-Cenozoic basaltic volcanism in eastern China. *Geological Journal of China Universities* **11**, 9–46.

Pan FB, Zhang HF, Xu WC, Guo L, Luo BJ and Wang S (2016) U–Pb zircon dating, geochemical and Sr–Nd–Hf isotopic compositions of Motuo quartz–monzonite: implication for the genesis and diversity of the high Ba–Sr granitoids in orogenic belt. *Tectonophysics* **668–669**, 52–64.

Peng TP, Wang YJ, Guo F and Peng BX (2004) SHRIMP zircon U-Pb geochronology of the diorites for southern Taihang Mountains in the North China Interior and its petrogenesis. *Acta Petrologica Sinica* **5**, 264–73 (in Chinese with English abstract).

Qian Q, Chung SL, Li TY and Wen DR (2002) Geochemical characteristics and petrogenesis of the Badaling high Ba-Sr granitoids: a comparison of igneous rocks from North China and the Dabie-Sulu Orogen. *Acta Petrologica Sinica* **18**, 275–92 (in Chinese with English abstract).

Qian Q and Hermann J (2010) Formation of high-Mg diorites through assimilation of peridotite by monzodiorite magma at crustal depths. *Journal of Petrology* **51**, 1381–416.

Richards JP and Kerrich R (2007) Adakite-like rocks: their diverse origins and questionable role in metallogenesis. *Economic Geology* **102**, 537–76.

Rudnick RL (1995) Making continental crust. *Nature* **378**, 571–7.

Rudnick RL, McDonough WF and Chappell BW (1993) Carbonatite metasomatism in the northern Tanzanian mantle: petrographic and geochemical characteristics. *Earth and Planetary Science Letters* **114**, 463–75.

Scherer E, Münker C and Mezger K (2001) Calibration of the lutetium-hafnium clock. *Science* **293**, 683–7.

Seton M, Müller RD, Zahirovic S, Gaina C, Torsvik T, Shephard G, Talsma A, Gurnis M, Turner M and Maus S (2012) Global continental and ocean basin reconstructions since 200 Ma. *Earth-Science Reviews* **113**, 212–70.

Shen JF, Santosh M, Li SR, Zhang HF, Yin N, Dong GC, Wang YJ, Ma GG and Yu HJ (2013) The Beiminghe skarn iron deposit, eastern China: geochronology, isotope geochemistry and implications for the destruction of the North China Craton. *Lithos* **156–159**, 218–29.

Sláma J, Košler J, Condon DJ, Crowley JL, Gerdes A, Hanchar JM, Horstwood MSA, Morris GA, Nasdala L, Norberg N, Schaltegger U, Schoene B, Tubrett MN and Whitehouse MJ (2008) Plešovice zircon: a new natural reference material for U–Pb and Hf isotopic microanalysis. *Chemical Geology* **249**, 1–35.

Spera FJ and Bohrson WA (2001) Energy-constrained open-system magmatic processes I: general model and energy-constrained assimilation and fractional crystallization (EC-AFC) formulation. *Journal of Petrology* **42**, 999–1018.

Sun Y, Xiao L, Zhan QY, Wu JX, Zhu D, Huang W, Bai M and Zhang YH (2015) Petrogenesis of the Kuangshancun and Hongshan intrusive complexes from the Handan–Xingtai district: implications for iron mineralization associated with Mesozoic magmatism in the North China Craton. *Journal of Asian Earth Sciences* **113**, 1162–78.

Sun Y, Xiao L, Zhu D, Wu T, Deng X, Bai M and Wen G (2014) Geochemical, geochronological, and Sr–Nd–Hf isotopic constraints on the petrogenesis of the Qicun intrusive complex from the Handan–Xingtai district: implications for the mechanism of lithospheric thinning of the North China Craton. *Ore Geology Reviews* **57**, 363–74.

Tang YJ, Zhang HF, Ying JF, Su BX, Chu ZY, Xiao Y and Zhao XM (2013) Highly heterogeneous lithospheric mantle beneath the Central Zone of the North China Craton evolved from Archean mantle through diverse melt refertilization. *Gondwana Research* **23**, 130–40.

Tarney J and Jones CE (1994) Trace element geochemistry of orogenic igneous rocks and crustal growth models. *Journal of the Geological Society* **151**, 855–68.

Thirlwall MF (1991) Long-term reproducibility of multicollector Sr and Nd isotope ratio analysis. *Chemical Geology: Isotope Geoscience section* **94**, 85–104.

Vervoort JD and Blichert-Toft J (1999) Evolution of the depleted mantle: Hf isotope evidence from juvenile rocks through time. *Geochimica et Cosmochimica Acta* **63**, 533–56.

Wang H, Xu Z, Lu X, Fu B, Lu J, Yang X and Zhao Z (2016*a*) Two-types of Early Cretaceous adakitic porphyries from the Luxi terrane, eastern North China Block: melting of subducted Paleo-Pacific slab and delaminated newly underplated lower crust. *Lithos* **240–243**, 140–54.

Wang YJ, Fan WM, Zhang HF and Peng TP (2006) Early Cretaceous gabbroic rocks from the Taihang Mountains: implications for a paleosubduction-related lithospheric mantle beneath the central North China Craton. *Lithos* **86**, 281–302.

Wang YM, Huang JS and Zhong SJ (2015) Episodic and multistaged gravitational instability of cratonic lithosphere and its implications for reactivation of the North China Craton. *Geochemistry, Geophysics, Geosystems* **16**, 815–33.

Wang YM, Huang JS, Zhong SJ and Chen JM (2016*b*) Heat flux and topography constraints on thermochemical structure below North China Craton regions and implications for evolution of cratonic lithosphere. *Journal of Geophysical Research: Solid Earth* **121**, 3081–98.

Wang YY, Zeng LS, Chen FK, Cai JH, Yan GH, Hou KJ and Wang Q (2017) The evolution of high Ba-Sr granitoid magmatism from "crust-mantle" interaction: a record from the Laoshan and Huyanshan complexes in the central North China Craton. *Acta Petrologica Sinica* **33**, 3873–96 (in Chinese with English abstract).

Wang ZL, Yang LQ, Deng J, Santosh M, Zhang HF, Liu Y, Li RH, Huang T, Zheng XL and Zhao H (2014) Gold-hosting high Ba-Sr granitoids in the Xincheng gold deposit, Jiaodong Peninsula, East China: petrogenesis and tectonic setting. *Journal of Asian Earth Sciences* **95**, 274–99.

Windley BF, Maruyama S and Xiao WJ (2010) Delamination/thinning of sub-continental lithospheric mantle under Eastern China: the role of water and multiple subduction. *American Journal of Science* **310**, 1250–93.

Wu FY, Lin JQ, Wilde SA, Zhang XO and Yang JH (2005) Nature and significance of the Early Cretaceous giant igneous event in eastern China. *Earth and Planetary Science Letters* **233**, 103–19.

Wu FY, Walker RJ, Yang YH, Yuan HL and Yang JH (2006) The chemical-temporal evolution of lithospheric mantle underlying the North China Craton. *Geochimica et Cosmochimica Acta* **70**, 5013–34.

Xu JF, Shinjo R, Defant MJ, Wang Q and Rapp RP (2002) Origin of Mesozoic adakitic intrusive rocks in the Ningzhen area of east China: partial melting of delaminated lower continental crust? *Geology* **30**, 1111–14.

Xu WL, Yang DB, Gao S, Pei FP and Yu Y (2010) Geochemistry of peridotite xenoliths in Early Cretaceous high-Mg# diorites from the Central Orogenic Block of the North China Craton: the nature of Mesozoic lithospheric mantle and constraints on lithospheric thinning. *Chemical Geology* **270**, 257–73.

Xu WL, Yang DB, Pei FP and Yu Y (2009*b*) Petrogenesis of Fushan high-Mg# diorites from the southern Taihang Mrs. in the central North China Craton: resulting from interaction of peridotite-melt derived from partial melting of delaminated lower continental crust. *Acta Petrologica Sinica* **25**, 1947–61 (in Chinese with English abstract).

Xu WL, Zhou QJ, Pei FP, Yang DB, Gao S, Li QL and Yang YH (2013) Destruction of the North China Craton: delamination or thermal/chemical erosion? Mineral chemistry and oxygen isotope insights from websterite xenoliths. *Gondwana Research* **23**, 119–29.

Xu YG (2007) Diachronous lithospheric thinning of the North China Craton and formation of the Daxin'anling-Taihangshan gravity lineament. *Lithos* **96**, 281–98.

Xu YG, Li HY, Hong LB, Ma L, Ma Q and Sun MD (2018) Generation of Cenozoic intraplate basalts in the big mantle wedge under eastern Asia. *Science China Earth Sciences* **61**, 869.

Xu YG, Li HY, Pang CJ and He B (2009*a*) On the timing and duration of the destruction of the North China Craton. *Chinese Science Bulletin* **54**, 3379–96.

Yang DB, Xu WL, Zhao GC, Huo TF, Shi JP and Yang HT (2016) Tectonic implications of Early Cretaceous low-Mg adakitic rocks generated by partial melting of thickened lower continental crust at the southern margin of the central North China Craton. *Gondwana Research* **38**, 220–37.

Yang JH, O'Reilly SY, Walker RJ, Griffin WL, Wu FY, Zhang M and Pearson N (2010) Diachronous decratonization of the Sino-Korean craton: geochemistry of mantle xenoliths from North Korea. *Geology* **38**, 799–802.

Ye HM, Li XH, Li ZX and Zhang CL (2008) Age and origin of high Ba–Sr appinite–granites at the northwestern margin of the Tibet Plateau: implications for early Paleozoic tectonic evolution of the Western Kunlun orogenic belt. *Gondwana Research* **13**, 126–38.

Ying JF, Zhang HF and Tang YJ (2011) Crust–mantle interaction in the central North China Craton during the Mesozoic: evidence from zircon U–Pb

https://doi.org/10.1017/S0016756819000256 Published online by Cambridge University Press

chronology, Hf isotope and geochemistry of syenitic–monzonitic intrusions from Shanxi province. *Lithos* **125**, 449–62.

Zhai MG, Fan QC, Zhang HF, Sui JL and Shao JA (2007) Lower crustal processes leading to Mesozoic lithospheric thinning beneath eastern North China: underplating, replacement and delamination. *Lithos* **96**, 36–54.

Zhang HF (2009) Peridotite-melt interaction: a key point for the destruction of cratonic lithospheric mantle. *Chinese Science Bulletin* **54**, 3417–37.

Zhang HF, Sun M, Zhou XH and Ying JF (2005) Geochemical constraints on the origin of Mesozoic alkaline intrusive complexes from the North China Craton and tectonic implications. *Lithos* **69**, 297–317.

Zhang HF, Zhu RX, Santosh M, Ying JF, Su BX and Hu Y (2013) Episodic widespread magma underplating beneath the North China Craton in the Phanerozoic: implications for craton destruction. *Gondwana Research* **23**, 95–107.

Zhang Q, Wang Y, Qian Q, Yang JH, Wang YL, Zhao TP and Guo GJ (2001) The characteristics and tectonic-metallogenic significances of the adakites in Yanshan period from eastern China. *Acta Petrologica Sinica* **17**, 236–44 (in Chinese with English abstract).

Zhang SH, Zhao Y, Davis GA, Ye H and Wu F (2014) Temporal and spatial variations of Mesozoic magmatism and deformation in the North China Craton: implications for lithospheric thinning and decratonization. *Earth-Science Reviews* **131**, 49–87.

Zhao DP, Maruyama S and Omori S (2007) Mantle dynamics of Western Pacific and East Asia: insight from seismic tomography and mineral physics. *Gondwana Research* **11**, 120–31.

Zhao GC and Cawood PA (2012) Precambrian geology of China. *Precambrian Research* **222–223**, 13–54.

Zheng JM, Xie GQ, Liu J, Chen MH, Wang SM, Guo SF, Ga X and Li GD (2007*b*) ^{40}Ar-^{39}Ar dating of phologopite from the Xishimen skarn iron deposit in the Handan-Xingtai area, southern Hebei, and its implications. *Acta Petrologica Sinica* **23**, 2513–18 (in Chinese with English abstract).

Zheng JP (2009) Comparison of mantle-derived materials from different spatiotemporal settings: implications for destructive and accretional processes of the North China Craton. *Chinese Science Bulletin* **54**, 3397–416.

Zheng JP, Griffin WL, O'Reilly SY, Yang JS, Li TF, Zhang M, Zhang RY and Liou JG (2006) Mineral chemistry of peridotites from Paleozoic, Mesozoic and Cenozoic lithosphere: constraints on mantle evolution beneath Eastern China. *Journal of Petrology* **47**, 2233–56.

Zheng JP, Griffin WL, O'Reilly SY, Yu CM, Zhang HF, Pearson N and Zhang M (2007*a*) Mechanism and timing of lithospheric modification and replacement beneath the eastern North China Craton: peridotitic xenoliths from the 100 Ma Fuxin basalts and a regional synthesis. *Geochimica et Cosmochimica Acta* **71**, 5203–25.

Zheng JP, O'Reilly SY, Griffin WL, Lu FX, Zhang M and Pearson NJ (2001) Relict refractory mantle beneath the eastern North China block: significance for lithosphere evolution. *Lithos* **57**, 43–66.

Zheng YF, Xu Z, Zhao ZF and Dai LQ (2018) Mesozoic mafic magmatism in North China: implications for thinning and destruction of cratonic lithosphere. *Science China Earth Sciences* **61**, 353–85.

Zhu J, Li QG, Chen X, Tang HS, Wang ZQ, Chen YJ, Liu SW, Xiao B and Chen JL (2018) Geochemistry and petrogenesis of the early Palaeozoic appinite-granite complex in the Western Kunlun Orogenic Belt, NW China: implications for Palaeozoic tectonic evolution. *Geological Magazine* **155**, 1641–66.

Zhu RX, Yang JH and Wu FY (2012) Timing of destruction of the North China Craton. *Lithos* **149**, 51–60.